

# Galaxy clustering and projected density profiles as traced by satellites in photometric surveys: Methodology and luminosity dependence

Wenting Wang<sup>1,2</sup>, Y.P. Jing<sup>1</sup>, Cheng Li<sup>1</sup>, Teppei Okumura<sup>3,1</sup>, Jiaxin Han<sup>1,2</sup>

## ABSTRACT

We develop a new method which measures the projected density distribution  $w_p(r_p)n$  of photometric galaxies surrounding a set of spectroscopically-identified galaxies, and simultaneously the projected cross-correlation function  $w_p(r_p)$  between the two populations. In this method we are able to divide the photometric galaxies into subsamples in luminosity intervals even when redshift information is unavailable, enabling us to measure  $w_p(r_p)n$  and  $w_p(r_p)$  as a function of not only the luminosity of the spectroscopic galaxy, but also that of the photometric galaxy. Extensive tests show that our method can measure  $w_p(r_p)$  in a statistically unbiased way. The accuracy of the measurement depends on the validity of the assumption inherent to the method that the foreground/background galaxies are randomly distributed and are thus uncorrelated with those galaxies of interest. Therefore, our method can be applied to the cases where foreground/background galaxies are distributed in large volumes, which is usually valid in real observations.

We have applied our method to data from the Sloan Digital Sky Survey (SDSS) including a sample of  $10^5$  luminous red galaxies (LRGs) at  $z \sim 0.4$  and a sample of about half a million galaxies at  $z \sim 0.1$ , both of which are cross-correlated with a deep photometric sample drawn from the SDSS. On large scales, the relative bias factor of galaxies measured from  $w_p(r_p)$  at  $z \sim 0.4$  depends on luminosity in a manner similar to what is found for those at  $z \sim 0.1$ , which are usually probed by autocorrelations of spectroscopic samples in previous studies. On scales smaller than a few Mpc and at both  $z \sim 0.4$  and  $z \sim 0.1$ , the photometric galaxies of different luminosities exhibit similar density profiles around spectroscopic galaxies at fixed luminosity and redshift. This provides clear observational support for the assumption commonly-adopted in halo occupation distribution (HOD) models that satellite galaxies of different luminosities are distributed in a similar way, following the dark matter distribution within their host halos.

---

<sup>1</sup>Key Laboratory for Research in Galaxies and Cosmology of Chinese Academy of Sciences, Max-Panck-Institute Partner Group, Shanghai Astronomical Observatory, Nandan Road 80, Shanghai 200030, China

<sup>2</sup>Graduate School of the Chinese Academy of Sciences, 19A, Yuquan Road, Beijing, China

<sup>3</sup>Institute for the Early Universe, Ewha Womans University, Seoul, 120-750, Korea

## 1. INTRODUCTION

In cold dark matter dominated cosmological models, dark matter halos form in density peaks in the universe under the influence of gravity, and thus are clustered in a different way from the underlying dark matter. In other words, they are *biased* in spatial distribution relative to dark matter (e.g. Mo & White 1996; Jing 1998; Seljak & Warren 2004). Galaxies are believed to form inside these halos (White & Rees 1978), and thus their spatial distribution is also biased with respect to dark matter (e.g. Kaiser 1984; Davis et al. 1985; Bardeen et al. 1986). On large scales ( $\gtrsim 10\text{Mpc}$ ), such biasing is nearly linear and the clustering of dark matter is well described by linear perturbation theory. On smaller scales, in contrast, galaxies do not trace dark matter simply. Complicated physical processes involved in galaxy formation and evolution have to be considered if one desires to fully understand galaxy clustering (e.g. White & Frenk 1991; Kauffmann et al. 1999; Colberg et al. 2000). This leads galaxy clustering and biasing to depend on a variety of factors including spatial scale, redshift and galaxy properties. Therefore measuring the clustering of galaxies as a function of their physical properties over large ranges in spatial scale and redshift is helpful for understanding how galaxies have formed and evolved.

Recent large redshift surveys, in particular the Two Degree Field Galaxy Redshift Survey (Colless et al. 2001, 2dFGRS) and the Sloan Digital Sky Survey (York et al. 2000, SDSS), have enabled detailed studies on galaxy clustering in the nearby universe. These studies have well established that the clustering of galaxies depends on a variety of properties, such as luminosity, stellar mass, color, spectral type, and morphology (Norberg et al. 2001, 2002; Madgwick et al. 2003; Zehavi et al. 2002, 2005; Goto et al. 2003; Li et al. 2006; Zehavi et al. 2010). More luminous (massive) galaxies are found to cluster more strongly than less luminous (massive) galaxies, with the luminosity (mass) dependence being more remarkable for galaxies brighter than  $L_*$  (the characteristic luminosity of galaxy luminosity function described by a Schechter function, Schechter (1976)). Moreover, galaxies with redder colors, older stellar populations and more bulge-dominated structure show higher clustering amplitudes and steeper slopes in their two-point correlation functions.

There have also been recent studies on galaxy clustering at higher redshifts. At  $z \sim 1$ , the DEEP2 Galaxy Redshift Survey (Davis et al. 2003) and the VIMOS-VLT Deep Survey (Le Fèvre et al. 2005, VVDS) have shown that galaxy clustering depends on luminosity, stellar mass, color, spectral type and morphology, largely consistent with what are found for the local universe (Coil et al. 2004, 2006; Meneux et al. 2006; Coil et al. 2008; Meneux et al. 2008; de la Torre et al. 2009). In contrast, the zCOSMOS survey (Lilly et al. 2007) shows no clear luminosity dependence of galaxy clustering over redshift range  $0.2 \leq z \leq 1$  (Meneux et al. 2009). More surprisingly, the projected two-point auto-correlation function  $w_p(r_p)$  derived from the zCOSMOS is significantly higher and flatter than from the VVDS (Meneux et al. 2008, 2009).

The observational measurements of galaxy clustering at both  $z \sim 0$  and  $z \sim 1$  as described above have been widely used to test theories of galaxy formation (e.g. Kauffmann et al. 1997; Benson et al. 2000; Li et al. 2007; Guo et al. 2010), as well as to quantify the evolution of galaxy

clustering from high to low redshifts (e.g. Zheng et al. 2007; Meneux et al. 2008; Wang & Jing 2010). Galaxy clustering has also been used to constrain halo occupation distribution(HOD) models, which provide statistical description on how galaxies are linked to their host halos and hence useful clues for understanding galaxy formation (e.g., Jing et al. 1998; Jing & Boerner 1998; Peacock & Smith 2000; Ma & Fry 2000; Seljak 2000; Scoccimarro et al. 2001; Berlind & Weinberg 2002; Cooray & Sheth 2002; Yang et al. 2003; Zheng et al. 2005; Tinker et al. 2005).

At intermediate redshifts ( $0.2 \lesssim z \lesssim 1$ ), progress on measuring galaxy clustering has been relatively hampered by the lack of suitable data sets. A few studies (e.g. Shepherd et al. 2001; Carlberg et al. 2001; Firth et al. 2002; Phleps et al. 2006) have measured galaxy clustering as a function of color which are in broad agreement with results found for the local universe. However, the dependence of clustering on luminosity, which is well seen in the local universe, has not been fully established at these intermediate redshifts, very likely due to the limited size of the spectroscopic samples. These samples usually cover small area on the sky, suffering from both sampling noise and large-scale structure noise (the so-called *cosmic variance* effect).

In this paper, rather than measuring the *auto-correlation* of these galaxies as in most previous studies, we develop a new method for estimating the projected two-point *cross-correlation function*  $w_p(r_p)$  between a given set of spectroscopically identified galaxies and a large sample of photometric galaxies. In brief, we first estimate the angular cross-correlation function between the spectroscopic and the photometric samples. We then determine the projected, average number density distribution  $w_p(r_p)n$  of the photometric galaxies surrounding the spectroscopic objects, as well as the projected two-point cross-correlation function  $w_p(r_p)$ . The photometric sample is usually the parent sample of the spectroscopic galaxies, but goes to much fainter limiting magnitudes. The spectroscopic sample could be clusters (or groups) of galaxies, central galaxies of dark matter halos such as the luminous red galaxies (LRGs) in the SDSS, quasars, or any spectroscopic galaxy populations of interest. Our method can yield a measurement of the projected density distribution of galaxies with certain physical properties (such as luminosity, color, etc.) around spectroscopic objects of certain properties. In this paper we focus on presenting our methodology and limit the application to galaxies of different luminosities. We plan to examine the dependence of  $w_p(r_p)n$  and  $w_p(r_p)$  on other properties (color, morphology, etc.) in future work.

Previous studies of satellite galaxy distribution around relatively bright galaxies are mostly limited to low redshifts ( $z < 0.1$ , e.g. Lake & Tremaine 1980; Phillipps & Shanks 1987; Vader & Sandage 1991; Lorrimer et al. 1994; Sales & Lambas 2005; Chen et al. 2006). Masjedi et al. (2006) and Zehavi et al. (2005) have recently investigated cross-correlations between spectroscopic and imaging galaxy samples at intermediate redshift ( $0.2 \lesssim z \lesssim 0.4$ ), but with different methods and focuses. Here we apply our method to a deep, photometric galaxy catalogue and a spectroscopic LRG sample at  $z \sim 0.4$ , both of which are drawn from the final data release of the SDSS (Abazajian et al. 2009). The LRGs are expected to be the central galaxy of their host dark matter halos. Therefore, by measuring  $w_p(r_p)n$  on scales smaller than a few Mpc, we yield an estimate of the density distribution of satellites galaxies within their host halo, as well as its dependence on luminosities of

both central and satellite galaxies. On larger scales, our analysis leads to a measurement of linear relative bias factor for photometric galaxies of different luminosities.

We describe our galaxy samples in § 2 and present our methodology in § 3. Applications to SDSS data are presented in § 4. We summarize and discuss in the last section. Throughout this paper we assume a cosmology with  $\Omega_m = 0.3, \Omega_\Lambda = 0.7$  and  $H_0 = 100h \text{ km s}^{-1} \text{ Mpc}^{-1}$  ( $h = 1$ ).

## 2. Data

### 2.1. The LRG sample at intermediate redshift

The LRG sample is constructed from the SDSS data release 7 (DR7 Abazajian et al. 2009), consisting of 101,658 objects with spectroscopically measured redshift in the range  $0.16 < z < 0.47$ , absolute magnitude limited to  $-23.2 < M_{0.3g} < -21.2$  and redshift confidence parameter greater than 0.95. Here  $M_{0.3g}$  is the  $g$ -band absolute magnitude  $K$ - and  $E$ -corrected to redshift  $z = 0.3$  (see Eisenstein et al. 2001 for references). We further select those LRGs that are expected to be the central galaxy of their host dark matter halos, using a method similar to that adopted in Reid & Spergel (2009) and Okumura et al. (2009). We use linking lengths of  $0.8 h^{-1} \text{ Mpc}$  and  $20 h^{-1} \text{ Mpc}$  for separations perpendicular and parallel to the line of sight when linking galaxies into groups. This leads to a total of 93802 central galaxies (about 92.3% of the initial LRG catalogue), covering a sky area which is almost the same as that of Kazin et al. (2010). From this catalogue we select five samples in two luminosity intervals ( $-23.2 < M_{0.3g} < -21.8$  and  $-21.8 < M_{0.3g} < -21.2$ ) and in three redshift intervals ( $0.16 < z < 0.26$ ,  $0.26 < z < 0.36$  and  $0.36 < z < 0.46$ ). Details of our samples are listed in Table 1. These samples so selected are volume limited, except **Sample L4** which is approximately, but not perfectly volume limited as can be seen from fig. 1 of Zehavi et al. (2005). Figure 1 shows the redshift distributions of our LRGs in the two luminosity intervals.

### 2.2. The low-redshift galaxy sample

Our spectroscopic galaxy sample in the local Universe is constructed from the New York University Value Added Galaxy Catalog (NYU-VAGC)<sup>4</sup>, which is built by Blanton et al. (2005) based on the SDSS DR7. From the NYU-VAGC we select a magnitude-limited sample of 533,731 objects with  $0.001 < z < 0.5$  and  $r$ -band Petrosian magnitude in the range  $10.0 < r < 17.6$ . The sample has a median redshift of  $z = 0.09$ , with the majority of the galaxies at  $z < 0.25$ . The galaxies are divided into five non-overlapping redshift bins, ranging from  $z = 0.03$  to  $z = 0.23$  with an equal interval of  $\Delta z = 0.04$ . The galaxies in each redshift bin are further restricted to various luminosity ranges, giving rise to a set of eight volume limited samples as listed in Table 2. The  $r$ -

---

<sup>4</sup><http://sdss.physics.nyu.edu/vagc/>

band absolute magnitude  $M_{0.1r}$  is  $K$ - and  $E$ -corrected to its value at  $z = 0.1$  following Blanton et al. (2003) (hereafter B03). Figure 2 shows the redshift distribution of the galaxies falling into the three luminosity ranges which are used to select the samples. These samples by construction are at lower redshifts when compared to the LRG samples, allowing us to make use of photometric galaxies for our analysis over wide ranges in luminosity and redshift. We don’t attempt to select central galaxies as done for LRGs above, as it is not straightforward to do so. Thus one should keep in mind that by using the low-redshift samples selected here we will measure density profiles and projected correlations for general populations of galaxies, not only for central galaxies.

### 2.3. The photometric galaxy sample and random samples

We construct our photometric galaxy sample from the **datasweep** catalogue which is included as a part of the NYU-VAGC. This is a compressed version of the full photometric catalogue of the SDSS DR7 that was used by Blanton et al. (2005) to build the NYU-VAGC. It contains only decent detections and includes a subset of all photometric quantities, which is enough for our analysis. Starting from the datasweep catalogue, we select all galaxies with  $r$ -band apparent Petrosian magnitudes in the range  $10 < r < 21$  after a correction for Galactic extinction and with point spread function and model fluxes satisfying  $f_{model} > 0.875 \times f_{PSF}$  in all five bands. In order to select unique objects in a run that are not at the edge of the field, we require the `RUN PRIMARY` flag to be set and the `RUN EDGE` flag not to be set. Finally we also require the galaxies to be located within *target tiles* of the Legacy Survey (Blanton et al. 2003). This procedure results in a sample of  $\sim 21.1$  million galaxies.

As shown by Ross et al. (2007), the datasweep catalogue needs to be properly masked, otherwise the angular correlation function obtained would be falsely flat on large scales. We describe the SDSS imaging geometry in terms of disjoint spherical polygons (Hamilton & Tegmark 2002; Tegmark et al. 2002; Blanton et al. 2005), which accompany the NYU-VAGC release and are available from the NYU-VAGC website. We exclude all polygons (and thus the galaxies located within them) which contain any object with seeing greater than  $1.5''$  or Galactic extinction  $A_r > 0.2$ . We also exclude polygons that intersect the mask for galaxy M101 as described in Ross et al. (2007). As a result, a fraction of about 14.32% of the total survey area has been discarded, slightly larger than in Ross et al. (2007) where the authors exclude image pixels rather than polygons with less critical criteria than adopted here. We also restrict ourselves to galaxies located in the main contiguous area of the survey in the northern Galactic cap, excluding the three survey strips in the southern cap (about 10 per cent of the full survey area). These restrictions result in a final sample of  $\sim 19.7$  million galaxies.

We have constructed a random sample which has exactly the same geometry and limiting magnitudes as the real photometric sample. This is done by generating sky positions (RA and Dec) at random within the polygons covering the real galaxies. In this work both the photometric sample and the random sample are cross-correlated with a given spectroscopic sample to estimate the

two-point angular cross-correlation function  $w(\theta)$  between the spectroscopic and the photometric samples.

### 3. Methodology

In our method we estimate in the first place the angular cross-correlation function  $w(\theta)$  between a given set of spectroscopic galaxies selected by luminosity and redshift (samples listed in Tables 1 and 2) and a set of photometric galaxies that, if they were at the redshift of the spectroscopic sample, would be expected to fall in a given luminosity range. Next, we convert  $w(\theta)$  to determine the projected density distribution  $w_p(r_p)n$  of the photometric galaxies around the spectroscopic galaxies, from which we further estimate the projected cross-correlation function  $w_p(r_p)$  between the two populations. In this section we describe how we select photometric galaxies in a given luminosity range, followed by description of our measures of  $w(\theta)$  as well as the way of determining  $w_p(r_p)n$  and  $w_p(r_p)$ .

#### 3.1. Selecting photometric galaxies according to luminosity and redshift

Considering a sample of spectroscopic galaxies with absolute magnitude and redshift in the ranges  $M_{s,1} < M_s < M_{s,2}$  and  $z_1 < z_s < z_2$ , we want to measure the cross-correlation of this sample with a set of photometric galaxies with absolute magnitude  $M_{p,1} < M_p < M_{p,2}$ . Due to the lack of redshift information for the photometric sample, it is not straightforward to determine which galaxies should be selected in order to have a subset falling in the expected luminosity range. One can overcome this difficulty by the fact that the cross-correlation signal is dominated by those photometric galaxies that are at the same redshifts as the spectroscopic objects, while both foreground (below  $z_1$ ) and background (above  $z_2$ ) galaxies contribute little. This is reasonably true when the redshift interval  $z_2 - z_1$  and the projected physical separation  $r_p$  in consideration are substantially small, for the clustering power decreases rapidly (approximately a power law) with increasing separation. On large scales, projection effect due to contamination of foreground and background galaxies becomes relatively large (we will discuss more about this point in § 3.3.1). With this assumption in mind we restrict ourselves to photometric galaxies with apparent magnitude  $m_{p,1} < m_p < m_{p,2}$ , the magnitude range for photometric galaxies to have absolute magnitude in the range  $M_{p,1} < M_p < M_{p,2}$  at redshift  $z_1 < z_p < z_2$ , when estimating angular cross-correlation functions.

When calculating the apparent magnitude for a given absolute magnitude and redshift, we have adopted the empirical formula of  $K$ -correction presented by Westra et al. (2010), which works at  $r$ -band as a function of observed  $g - r$  color and redshift. Since  $K$ -correction value changes slowly with redshift, we adopt  $(z_1 + z_2)/2$  as the input redshift value when applying the formula for simplicity. In this paper we adopt the  $^{0.1}r$ -band luminosity function from B03, and so we convert

the apparent magnitude in  $r$  to that in  $^{0.1}r$  using the analytical conversion formula provided by Blanton & Roweis (2007).

### 3.2. Measuring angular correlation functions

We use two estimators to measure the angular cross correlation function between a spectroscopic sample and a photometric sample. For small separations ( $\theta \lesssim 1000''$ ) we use the standard estimator (Davis & Peebles 1983)

$$w(\theta) = \frac{QD(\theta)}{QR(\theta)} - 1, \quad (1)$$

where  $\theta$  is the angular separation, and  $QD(\theta)$  and  $QR(\theta)$  are the cross pair counts between the spectroscopic sample and the photometric sample, and between the same spectroscopic sample and the random sample. Note that  $QR$  is normalized according to the ratio of the size of the photometric and random samples. For separations larger than  $\theta \sim 1000''$ , we instead use a Hamilton-like estimator (Hamilton 1993)

$$w(\theta) = \frac{QD(\theta)RR(\theta)}{QR(\theta)DR(\theta)} - 1, \quad (2)$$

where  $RR$  is the pair count of the random sample, and  $DR$  the cross pair count between the photometric and random samples. This estimator is expected to work better on large scales than the standard one, since it is less sensitive to uncertainties in the mean number density of photometric galaxies (Hamilton 1993). The two estimators differ in  $w(\theta)$  by 10% to 20% at  $\theta \sim 1000''$  in our cases. On smaller scales the two estimators give almost identical results, with difference at a few percent level and well within error bars. In order to reduce computation time, we apply the standard estimator to a random sample of 30 million points for separations  $\theta \lesssim 1000''$ , while a smaller sample of 0.9 million random points and the Hamilton-like estimator are used for larger separations.

### 3.3. Converting $w(\theta)$ to $w_p(r_p)n$ and $w(r_p)$

Given a measurement of  $w(\theta)$  we estimate the corresponding projected cross-correlation function  $w_p(r_p)$  and projected density profile  $w_p(r_p)n$  in the following two ways. In this subsection the photometric and spectroscopic galaxy samples being considered are named **Sample 1** and **Sample 2**, respectively.

### 3.3.1. Direct conversion from $w(\theta)$ to $w_p(r_p)$

The relation between angular correlation function  $w(\theta)$  and real space correlation function  $\xi(r)$  is given by (see Peebles 1980)

$$w(\theta) = \frac{\int_0^\infty x_1^2 x_2^2 dx_1 dx_2 a_1^3 a_2^3 n_1 n_2 \xi(r_{1,2})}{\mathcal{N}_1 \mathcal{N}_2}, \quad (3)$$

where  $a$  and  $x$  stands for scale factor and comoving distance respectively;  $r_{1,2}$  is the real space separation between Sample 1 and Sample 2 galaxies;  $\mathcal{N}_1$  and  $\mathcal{N}_2$  are the surface number densities of the two samples;  $n_1$  and  $n_2$  are their comoving spatial number densities. Taking  $n_2$  as a sum of Dirac delta functions, we have

$$n_2 = \sum_k \delta(\vec{r}_2 - \vec{r}_k), \quad (4)$$

where  $\vec{r}_k$  stands for galaxy positions in Sample 2. Thus Eqn. (3) becomes

$$w(\theta) = \frac{\Omega_1 \Omega_2 \sum_k \int_0^\infty x_1^2 x_2^2 dx_1 dx_2 a_1^3 a_2^3 n_1 \delta(\vec{r}_2 - \vec{r}_k) \xi(r_{1,2})}{N_1 N_2} \quad (5)$$

$$= \frac{\Omega_1 \sum_k \int_0^\infty x_1^2 dx_1 a_1^3 n_1 \xi(r_{1,k})}{N_1 N_2} \quad (6)$$

$$= \frac{\sum_k \int_0^\infty dN_1 / dz_1 \xi(r_{1,k}) dz_1}{N_1 N_2}, \quad (7)$$

where

$$r_{1,k} = \sqrt{r_1^2 + r_k^2 - 2r_1 r_k \cos(\theta)}, \quad (8)$$

and  $r_1$  and  $r_k$  are the comoving distances for galaxies in Sample 1 and the  $k$ th galaxy in Sample 2. Here  $N_1$  and  $N_2$  are the total number of objects in the two samples. Let  $N_k$  denote the number of galaxies with approximately the same distance  $r_k$  (or redshift  $z_k$ ) in Sample 2, then Eqn. (7) can be written as

$$w(\theta) = \frac{\sum_k N_k \int_0^\infty dN_1 / dz_1 \xi(r_{1,k}) dz_1}{N_1 N_2}. \quad (9)$$

If the redshift bin of Sample 2 is thin enough, all the galaxies within it can be regarded as at the same redshift. This gives rise to a much simplified relation between  $w(\theta)$  and  $\xi(r)$ :

$$w(\theta) = \frac{\int_0^\infty dN_1 / dz_1 \xi(r_{1,2}) dz_1}{N_1}. \quad (10)$$

On the other hand, the relation between  $w_p(r_p)$  and  $\xi(r)$  is known to be

$$w_p(r_p) = 2 \int_{r_p}^\infty \xi(r) \frac{r dr}{\sqrt{r^2 - r_p^2}} = \int_{z_l}^{z_u} \xi(r_{1,2}) \frac{dD}{dz_1} dz_1, \quad (11)$$

where  $D$  is the comoving distance of Sample 1 galaxy,  $r_p$  the projected physical separation,  $z_l$  and  $z_u$  the lower and upper limits of the redshift interval in consideration. If  $dN_1 / dz_1$  and  $dD / dz_1$



change sufficiently slowly with redshift when compared to  $\xi(r_{1,k})$  as a function of  $r_{1,k}$ , where  $r_{1,k}$  depends on  $z_1$ , we can take  $dN_1/dz_1$  and  $dD/dz_1$  out of the integral. Thus for a thin redshift bin the ratio between  $w(\theta)$  and  $w_p(r_p)$  is simply approximated by

$$\frac{w(\theta)}{w_p(r_p)} = \frac{dN_1/dz_1}{N_1 dD/dz_1} \Big|_{z_1=z_{med}}, \quad (12)$$

where  $r_p = 2D \sin(\frac{\theta}{2})$  and  $z_{med}$  is the median of the redshift range. In practice we instead calculate the ratio in the following way to take into account the redshift dependence (though very weak) of  $dN_1/dz_1$  and  $dN_2/dz_1$ :

$$\frac{w(\theta)}{w_p(r_p)} = \frac{\int_{z_l}^{z_u} \left( \frac{dN_1/dz_1}{N_1 dD/dz_1} \Big|_{z_1=z} \right) (dN_2/dz) dz}{\int_{z_l}^{z_u} (dN_2/dz) dz}. \quad (13)$$

We also require the angular separation  $\theta$  to change accordingly with fixed  $r_p$ , and thus in this way the angular separation of our measured  $w(\theta)$  changes with the redshift of spectroscopic galaxies when counting galaxy-galaxy pairs. To be more specific, the  $r_p$  considered here range from  $r_p \sim 0.1 \text{ Mpc}/h$  to  $r_p \sim 25 \text{ Mpc}/h$  for LRGs, and from  $r_p \sim 0.1 \text{ Mpc}/h$  to  $r_p \sim 20 \text{ Mpc}/h$  for galaxies in the low-redshift sample, with 13 and 12 intervals of equal size in logarithmic space. Quantities in the right side of Eqn. (13) are determined either from data catalogue directly ( $N_2$  and  $dN_2/dz$ ) or from the luminosity function analytically ( $dN_1/dz$ ).

In order to understand to what extent Eqn. (13) holds, we have performed two tests. In the first test, we calculate a linear power spectrum  $P_l(k)$  using the CMBFAST code for the cosmology adopted here (Seljak & Zaldarriaga 1996; Zaldarriaga et al. 1998; Zaldarriaga & Seljak 2000), from which we calculate the nonlinear power spectrum  $P_{nl}(k)$  following Peacock & Dodds (1996). The real-space correlation function  $\xi(r)$  is then obtained by Fourier transforming  $P_{nl}(k)$ . The amplitude of  $\xi(r)$  is arbitrarily given which has no effect on the ratio of  $w(\theta)$  and  $w_p(r_p)$ . Next, the redshift distribution  $dN_1/dz_1$  for Sample 1 galaxies in a certain magnitude range is calculated analytically from the luminosity function of B03. Using Eqn. (9) and (11) we determine  $w(\theta)$  and  $w_p(r_p)$  for this magnitude range, giving rise to the *true* value of their ratio which we denote as  $ratio_{true}$ . When integrating the right part of Eqn. (9) we fix  $r_p$  and let the binning of  $\theta$  vary accordingly. We also calculate an approximated value for the same ratio using Eqn. (13), which we denote as  $ratio_{analy}$  and compare to the true ratio in order to test the validity of Eqn. (13).

Figure 3 shows the relative difference between the approximated and the true values of the  $w(\theta)/w_p(r_p)$  ratio,  $(ratio_{analy} - ratio_{true})/ratio_{true}$ , for Sample 2 galaxies with  $0.07 < z_2 < 0.078$  and  $-23.0 < M_2 < -21.0$ , and Sample 1 galaxies in several absolute magnitude intervals (as indicated in each panel). The approximated ratio agrees quite well with the true value, at 1% accuracy or better, for separations  $r_p \lesssim 10 \text{ Mpc}$  and for all luminosities considered. The discrepancy increases at larger separations, but well below 3% level even at the largest scale probed ( $\sim 30 \text{ Mpc}$ ). This discrepancy mainly comes from the distant-observer approximation adopted here. The accuracy of

Eqn. (13) is expected to be better for higher redshifts where the distant-observer approximation works better. We thus conclude that our approximation in Eqn. (13) works at substantially high accuracies for our purpose.

A second test that we have done is to apply our method to spectroscopic samples. Simply speaking,  $w_p(r_p)$  for a spectroscopic sample can be measured with the redshift information. It can also be estimated with our method without using the redshift information for the photometric sample. By comparing the two  $w_p(r_p)$  estimates we are able to understand how well our method works. For simplicity we consider here a specific case in which a spectroscopic sample of given luminosity and redshift ranges is cross-correlated with spectroscopic (for the true  $w_p(r_p)$ ) or “photometric” (for the  $w_p(r_p)$  obtained by our method) galaxies in the same ranges. Thus the  $w_p(r_p)$  are reduced to auto-correlation functions.

The result of this test is shown in Figure 4, where we plot the true  $w_p(r_p)$  in blue curves and the approximated one in red for SDSS Main galaxies (left column) and LRGs (right column) at different luminosities and redshifts (indicated in each panel). For LRGs we see good agreement between the two measurements on all scales and at all redshifts probed (with the difference  $< 20\%$ ). A similar agreement is seen for the low-redshift samples of  $-20 < M_{0.1r} < -19$  and  $-21 < M_{0.1r} < -20$ . All these results are very encouraging.

However, there is large difference ( $\sim 50\%$ ) between the results of the two methods on large scales ( $> 5\text{Mpc}/h$ ) for the brightest ( $-22 < M_{0.1r} < -21$ ) low redshift sample. The deviation may be caused by a coincident correlation between foreground galaxies in the photometric sample and the spectroscopic sample. We have performed a further analysis by estimating the cross-correlation with the foreground, the background, and the right redshift interval separately, for three low-redshift spectroscopic samples (corresponding to the left-hand panels in Fig. 4). We find that the contamination comes mainly from the foreground for the brightest sample ( $-22 < M_{0.1r} < -21$ ), and from the background for the faintest sample ( $-20 < M_{0.1r} < -19$ ). For both samples, the projected cross-correlation  $w_p(r_p)$  with the foreground (for the brightest sample) or the background (for the faintest sample) shows weak dependence on scale. When compared to the true  $w_p(r_p)$ , the cross-correlation with the foreground/background is negligible on small scales,  $\sim 50\%$  smaller at  $\sim 10\text{Mpc}/h$  and compatible at  $\sim 20\text{Mpc}/h$ . This result clearly shows that the clustering pattern of the foreground/background can contaminate the angular cross correlation function stochastically. This also explains why we can measure the projected correlation function for the LRG sample accurately, because the foreground/background galaxies are in big cosmic volumes and thus have weak correlations themselves.

We conclude that the accuracy of our method relies on the key assumption that foreground/background galaxies have weak correlation with the spectroscopic galaxies. This assumption is valid for many real observations, especially for spectroscopic samples at intermediate or high redshift. This is why we can recover the project correlation function for LRG samples on all scales. For the low redshift samples, our method works for the sample of luminosity  $M_*$ , since the foreground/background

galaxies are relatively small in number compared with those at the redshift of the spectroscopic sample. For the bright low redshift sample, the foreground galaxies are located in a small volume and are more numerous, and their clustering pattern can bias the estimation of the projected function. This effect is smaller for small scales, which is the reason why we can measure the projected function accurately on scales smaller than  $\sim 1$  Mpc/h.

### 3.3.2. Indirect conversion through $w_p(r_p)n$

We propose a second method here for estimating  $w_p(r_p)$ . Rather than directly converting  $w(\theta)$  to  $w_p(r_p)$ , we first convert the former to a projected density profile  $w_p(r_p)n_1$ , from which we then estimate  $w_p(r_p)$  by calculating analytically the spatial number density  $n_1$  from the luminosity function.  $w_p(r_p)n_1$  is obtained as a byproduct without suffering from uncertainties in galaxy luminosity function.

In this method we estimate a *weighted* angular correlation function  $w(\theta)_{weight}$  instead of the traditional function  $w(\theta)$  as discussed above. This is measured using the same estimators given in Eqn. (1) and (2), except that each spectroscopic galaxy in Sample 2 is weighted by  $D^{-2}$ , inverse of the square of comoving distance for Sample 2 galaxies. It can be easily proved with Eqn. (13) that for a thin redshift interval of the spectroscopic sample (Sample 2),  $N_1 w(\theta)_{weight}/\Omega$  equals to the projected density profile  $w_p(r_p)n_1$ , i.e.,

$$w_p(r_p)n_1 = \frac{N_1 w(\theta)_{weight}}{\Omega}, \quad (14)$$

where  $N_1$  and  $n_1$  are the number and number density of photometric galaxies in Sample 1, and  $\Omega$  the total sky coverage of Sample 1. Given the projected density profile  $w_p(r_p)n_1$  estimated by Eqn. (14) as well as the spatial number density of galaxies  $n_1$  analytically calculated from the luminosity function, we finally estimate the projected correlation function  $w_p(r_p)$  by dividing  $w_p(r_p)n_1$  by  $n_1$ . We emphasize here the projected density profile  $w_p(r_p)n_1$  does not suffer from uncertainties in luminosity function, because all quantities in the right side of Eqn. (14) can be obtained from data.

To calculate  $n_1$ , we adopt the luminosity evolution model and the luminosity function at  $z = 0.1$  from B03 when doing calculation for spectroscopic galaxies at low redshifts (samples selected from the SDSS Main galaxy catalogue as listed in Table 2). Considering that the evolution model of B03 is based on low-redshift data ( $z \lesssim 0.25$ ), which might not be suitable for higher redshifts, we adopt the evolution model of Faber et al. (2007) (here after F07) for our LRG samples. Moreover, we need to convert the F07 model from  $B$ -band to the  $^{0.1}r$ -band at which our galaxies are observed. Assuming that the slope of the luminosity evolution doesn't depend on waveband, we obtain the  $^{0.1}r$ -band luminosity evolution model by simply shifting the amplitude of the  $B$ -band model from F07 so as to have an amplitude at  $z = 0.1$  which is equal to the amplitude of the  $^{0.1}r$ -band model of B03. In this manner the slopes of the two models remain unmodified, which are  $Q = -1.23$  for

F07 and -1.62 for B03 respectively (see their papers for details)<sup>5</sup>.

In conclusion, the projected cross-correlation function  $w_p(r_p)$  can be measured either from Eqn. (13) by direct conversion of  $w(\theta)$ , or from Eqn. (14) by indirect conversion through estimating  $w_p(r_p)n$ . After having made extensive comparisons, we found that the two methods give rise to almost identical results. In what follows we choose to use the second method only, as it simultaneously provides both  $w_p(r_p)$  and  $w_p(r_p)n$ .

### 3.4. Division and combination of redshift subsamples

In this subsection we address an important issue which we have ignored so far. As mentioned above, our method for selecting photometric galaxies according to luminosity and redshift is valid only when the redshift interval  $z_2 - z_1$  is small enough. However, the redshift intervals used to select our spectroscopic galaxy samples apparently do not satisfy this condition. For example, for a redshift range of  $0.16 < z < 0.26$  and an absolute magnitude interval of  $M_{p,2} - M_{p,1} = 0.5$ , the photometric galaxies selected will cover a much broader apparent magnitude range,  $m_{p,2} - m_{p,1} = 1.7$ .

Our solution is to further divide the galaxies in a given spectroscopic sample into a number of subsamples which are equally spaced in redshift (hereafter called redshift sub-shells). See Tables 1 and 2 for the number of redshift sub-shells adopted for our samples. For a given sample, we measure the weighted angular cross-correlation function  $w(\theta)_{weight}$  (see above) for each sub-shell separately by cross-correlating with galaxies selected from the photometric catalogue in the way described above according to the expected luminosity range and the redshift range of the sub-shell. Each  $w(\theta)_{weight}$  measurement is then converted to give the corresponding projected density profile  $w_p(r_p)n$  as well as the projected cross-correlation function  $w_p(r_p)$ , using the second method described above. Estimates of these quantities for the sub-shells are then averaged to give the estimates for their parent sample as a whole. In this procedure each sub-shell is weighted by  $V_i/\sigma_i^2$ , with  $V_i$  being the comoving volume covered by the  $i$ th sub-shell and  $\sigma_i^2$  the variance of  $w_p(r_p)n$  or  $w_p(r_p)$  of the sub-shell. In order to estimate  $\sigma_i$  we have generated 100 bootstrap samples for each sub-shell. The variance  $\sigma_i$  of a sub-shell is then estimated by the  $1\sigma$  scatter between all its bootstrap samples. This weighting scheme ensures the averaged  $w_p(r_p)n$  or  $w_p(r_p)$  to be determined largely by sub-shells with relatively large volume and high signal-to-noise ratio (S/N) measurements, thus effectively reducing the overall sampling noise and cosmic variance.

In order to increase the accuracy of our method, one may want to increase the number of sub-shells for a given redshift range, at the cost of increasing both the sampling noise and the large-scale structure noise (the *cosmic variance*). In practice, we split a spectroscopic sample into redshift sub-shells by requiring  $\Delta z/z \lesssim 0.1$ , where  $\Delta z$  is the thickness of the sub-shells and  $z$  is the mean redshift

---

<sup>5</sup>We have repeated our analysis for LRGs, adopting  $Q = -1.62$  instead of  $Q = -1.23$ , and obtained similar results.

of the sample. With this restriction the difference between  $m_2 - m_1$  and  $M_2 - M_1$  ranges from  $\sim 0.25$  occurring for low-redshift sub-shells to  $\sim 0.1$  for high-redshift ones. Extensive tests show that our results are robust to reasonable change of the thickness of sub-shells. For instance, taking **Sample L1** from Table 1 as the spectroscopic sample, the cross-correlation function measured by 10 sub-shells differs from the one of 5 sub-shells by at most 10% for photometric galaxies with  $-22 < M < -21.5$ , and by only about 3% for the faintest luminosity bin ( $-19.5 < M < -19.0$ ).

### 3.5. Error estimation

We estimate the error in the averaged  $w_p(r_p)n$  or  $w_p(r_p)$  by

$$\Delta = \begin{cases} \sqrt{\sigma^2 \times \frac{\chi^2}{\text{dof.}}} & \text{if } \frac{\chi^2}{\text{dof.}} > 1 \\ \sigma & \text{if } \frac{\chi^2}{\text{dof.}} \leq 1, \end{cases} \quad (15)$$

with

$$\sigma^2 = \sum_{i=1}^{N_{sub}} \frac{V_i^2}{\sigma_i^2} \bigg/ \left( \sum_{i=1}^{N_{sub}} \frac{V_i}{\sigma_i^2} \right)^2, \quad (16)$$

$$\chi^2/\text{dof.} = \frac{1}{N_{sub} - 1} \sum_{i=1}^{N_{sub}} (x_i - x_{avg})^2 \sigma_i^{-2}, \quad (17)$$

where the sum goes over all the sub-shells of a given spectroscopic sample;  $x_i$  is the measurement of  $w_p(r_p)n$  or  $w_p(r_p)$  of the  $i$ th sub-shell and  $x_{avg}$  the average measurement for all the sub-shells as a whole;  $N_{sub}$  is the number of sub-shells. Overall, Eqn. (15) should be able to include both the volume effect (through factor  $V_i$ ) and the sampling noise (through  $\sigma_i$ ), thus providing a reasonable estimate of the errors in our measurements. By weighting the error by  $\sqrt{\frac{\chi^2}{\text{dof.}}}$ , we mean to take into account the large variation from sub-shell to sub-shell in some cases.

To better understand the error contribution from different redshift sub-shells, we plot in Figure 5 the  $w_p(r_p)$  measurements for **Sample L1** listed in Table 1. Different panels correspond to photometric galaxies in different luminosity intervals. In each panel, we plot  $w_p(r_p)$  for all the five sub-shells with their redshift ranges indicated in the bottom-right panel. Error bars on the  $w_p(r_p)$  curves are estimated using the bootstrap resampling technique, i.e.  $\sigma_i$  in Eqn. (16) and (17). We see that, for photometric galaxies at fixed luminosity,  $w_p(r_p)$  measurements of different sub-shells are almost on top of each other, indicating that the scatter between sub-shells is fairly small. This again shows that the correlation functions measured with our method are insensitive to the number of redshift sub-shells.

We note that the overall error increases rapidly with luminosity at the bright end. This reflects not only the sampling noise of the small samples, but more importantly, also an effect of a huge foreground population which significantly suppresses the *angular* cross-correlation signals.

Letting  $w'(\theta)$  be the angular correlation function between a spectroscopic sample with  $z_1 < z < z_2$  and a photometric sample including galaxies of all redshifts, and  $w(\theta)$  the one between the same spectroscopic sample and a sample of photometric galaxies within  $z_1 < z < z_2$ , one can easily show that

$$w'(\theta) = \frac{N_{GS}}{N_G} w(\theta), \quad (18)$$

where  $N_G$  and  $N_{GS}$  are respectively the number of photometric galaxies in the full sample and in the redshift range  $z_1 < z < z_2$ . In this case the estimated correlation signal is suppressed by a factor of  $\frac{N_{GS}}{N_G}$ , a large effect in particular when  $N_G \gg N_{GS}$  as in bright samples.

This is explained more clearly in Figure 6 where we plot the redshift distribution as calculated using the luminosity function of B03 for photometric galaxies which are selected according to luminosity and redshift using the method described in § 3.1. Plotted in different lines are the distributions for different luminosity ranges with redshift range fixed to  $0.2 < z < 0.22$ . According to our method of dividing photometric sample into luminosity subsamples, photometric galaxies selected to serve our purpose of a certain luminosity bin have the desired luminosity at the chosen redshift. As can be seen from the figure, in the brightest luminosity interval ( $-22.5 < M_{0.1r} < -22.0$ , solid line) only a small fraction of the galaxies are located within the expected redshift range, where the majority of galaxies are intrinsically fainter. It is this population that suppresses the angular cross-correlations that we measure at the bright end, leading to large uncertainties in  $w_p(r_p)$ , as seen in Figure 5.

Before we apply our method to SDSS data in the next section, we should point out that, although we have carefully considered both the sampling noise and the large-scale structure noise, our error estimation doesn't include the projection effect caused by background and foreground galaxies. Thus when interpreting our  $w_p(r_p)n$  and  $w_p(r_p)$  presented below, one should keep in mind that their errors are underestimated to varying degrees, depending on the redshift and luminosity we consider.

## 4. Applications to SDSS galaxies

### 4.1. Projected cross-correlations and density profiles of LRGs

In Figure 7 we show the projected density profile  $w_p(r_p)n$  for LRGs in different intervals of luminosity and redshift, as traced by surrounding photometric galaxies of different luminosities. Results are plotted for LRGs with  $-23.2 < M_{0.3g} < -21.8$  in panels on the left and for those with  $-21.8 < M_{0.3g} < -21.2$  on the right, with panels from top to bottom corresponding to different redshift bins. The  $w_p(r_p)n$  traced by photometric galaxies in different luminosity ranges are shown using different lines as indicated in the bottom-right panel. As can be seen, the projected number density of galaxies around central LRGs decreases as their luminosity increases. This is true for all redshifts and all scales probed. In particular, such luminosity dependence is weak for galaxies

fainter than the characteristic luminosity of the Schechter luminosity function ( $M_{0.1r} = -20.44$  for the SDSS), and becomes remarkable for brighter galaxies. The change of the amplitude mainly reflects the number density of galaxies as a function of their luminosity. From the figure one can easily read out the number of galaxies in the host halo of the LRGs. For example, on average there are about 3 galaxies of  $-20.5 < M < -20$  in the host halo of a LRG in **Sample L1**, assuming the host halo radius is  $0.3h^{-1}\text{Mpc}$ .

In Figure 8 we show projected cross-correlation function  $w_p(r_p)$  obtained from the  $w_p(r_p)n$  measurements shown in Figure 7, for the same set of LRG samples and the same intervals of photometric galaxy luminosity. At fixed scale and redshift, the amplitude of  $w_p(r_p)$  increases with increasing luminosity, a trend which has already been well established by previous studies. It is interesting to see from both figures that, although both  $w_p(r_p)n$  and  $w_p(r_p)$  show systematic trends with luminosity in amplitude, their slope remains fairly universal for given redshift and central galaxy luminosity, regardless of the luminosity of surrounding galaxies we consider. This provides direct observational evidence that satellite galaxies of different luminosities follow the distribution of dark matter in the same way within their dark matter halos, an assumption adopted in many previous studies on HOD modeling of galaxy distribution.

In Figure 9 we plot the  $w_p(r_p)$  again in order to explore the evolution with redshift. Measurements of different photometric galaxy luminosities are shown in different panels, while in each panel we compare  $w_p(r_p)$  measured at different redshifts for fixed luminosity. Note that in this figure we have considered the luminosity evolution of galaxies, as we aim to study how the projected density distribution and cross-correlation around the LRGs have evolved over the redshift range probed. We do not include  $E$ -correction in Figures 5, 7 and 8, because we want the results there to be less affected by possible uncertainty in the luminosity evolution model. From Figure 9, we see significant increase in the amplitude of  $w_p(r_p)$  as redshift goes from  $z = 0.4$  to  $0.2$ . Taking the  $-21.0 < M < -20.5$  bin in the left column for example, on average the  $w_p(r_p)$  amplitude differs by a factor of about 2 between the result of  $z \sim 0.2$  (blue curve) and  $z \sim 0.4$  (green curve) at separations  $r_p < 0.3h^{-1}\text{Mpc}$ , the typical boundary of LRG host halos.

It is important to understand whether the significant evolution seen above could be explained purely by evolution in dark matter distribution, or additional processes related to galaxies themselves are necessary. To the end we have done a simple calculation as follows. We assume that there is no merger occurring between galaxies or between their host halos. In this case all galaxies and halos have been evolving in a passive manner, and the total number of each keeps unchanged during the period in consideration. Thus galaxies at different redshifts are the same population which are hosted by the same set of halos. We calculate a dark matter density profile averaged over all dark matter halos that are expected to host LRGs of given redshift and luminosity, by

$$\rho_{avg}(r) = \frac{\int_{M_{min}}^{M_{max}} \rho(r, M) n(M) dM}{\int_{M_{min}}^{M_{max}} n(M) dM}, \quad (19)$$

where  $n(M)$  is the halo mass function from Sheth & Tormen (1999), and  $\rho(r, M)$  is the density

profile of halos of mass  $M$  assumed to be in the NFW form (Navarro et al. 1997). We determine the concentration parameter  $c$  of halos following Zhao et al. (2009). The lower and upper limits of halo mass ( $M_{min}$  and  $M_{max}$ ) are determined by matching the abundance of LRGs in our sample with that of dark matter halos given by the Sheth-Tormen mass function (Sheth & Tormen 1999). For this we have adopted the plausible assumption that the luminosity of a central galaxy is an increasing function of the mass of its halo.

We consider three redshifts which are  $z = 0.21, 0.31$  and  $0.41$ , approximately the median redshifts of our LRG samples. The dark matter density within  $0.3h^{-1}$  Mpc around LRGs of  $-23.2 < M_{0.3g} < -21.8$  is predicted to increase by 24.6% from  $z \sim 0.4$  to  $\sim 0.2$ , and 12.1% from  $z \sim 0.3$  and  $\sim 0.2$ . The factor is 10.6% for  $-21.8 < M_{0.3g} < -21.2$  from  $z \sim 0.3$  to  $\sim 0.2$ . It is clear that these predictions are much smaller when compared to what we have obtained from the SDSS data. As can be seen from Figure 9, at  $r_p < 0.3h^{-1}$  Mpc, the clustering amplitude changes by a factor of  $\sim 2$  between  $z \sim 0.4$  and  $\sim 0.2$ , and by 20 - 50% between  $z \sim 0.3$  and  $\sim 0.2$ .

This simple calculation seems to suggest that the evolution of galaxy clustering observed in this work is caused not only by the evolution of the underlying dark matter, but also by the evolution of galaxies themselves. However, this argument should not be overemphasized. As selected in  $r$ -band, our photometric sample may be biased to bluer galaxies as one goes to higher redshifts. This selection effect must be properly taken into account when one addresses the evolution of galaxy clustering, but such a detailed modeling is out of the scope of our current paper.

Figure 10 shows the relative bias factor of photometric galaxies with respect to  $L^*$  galaxies as a function of luminosity. Taking a LRG sample, the bias factor for a sample of photometric galaxies at given luminosity and redshift is calculated from the amplitude of the  $w_p(r_p)$  between the LRG and the photometric samples, normalized by the  $w_p(r_p)$  of the same LRG sample with a photometric sample selected by  $-21 < M_{0.1r} < -20$  ( $K$ - and  $E$ -corrected to  $z = 0.1$ )<sup>6</sup>, and averaged over separations between  $r_p = 2.5h^{-1}$  Mpc and  $10h^{-1}$  Mpc. The bias factor so obtained should be virtually identical to the one estimated from the auto-correlation function of the same set of photometric galaxies. In the figure, curves in different colors refer to results from different LRG samples in Table 1. Since the photometric sample becomes somewhat incomplete for  $L \lesssim L^*$  in the redshift range  $0.36 < z < 0.46$ , the bias factor for this sample (the green line in the figure) is normalized with respect to a  $-21.0 < M_{0.1r} < -20.5$  sample instead of the  $-21 < M_{0.1r} < -20$  one. Plotted in black triangles is the result of Li et al. (2006). Black dashed line is a fit obtained from the SDSS power spectrum by Tegmark et al. (2004). Relative bias factors at  $0.16 < z < 0.26$  (Samples L1 and L2) are well consistent with those previous studies at all luminosities, except the bright end where our measurement is slightly lower than that from Tegmark et al. (2004). Our bias factor measurements show that the luminosity dependence of galaxy clustering observed in the local Universe is very similar to that at intermediate redshift  $z \sim 0.4$ .

---

<sup>6</sup>The absolute magnitude range for selecting  $L^*$  samples varies from sub-shell to sub-shell for the photometric galaxies, so that the corresponding absolute magnitude range at  $z = 0.1$  is always  $-21 < M_{0.1r} < -20$ .



#### 4.2. Projected density profiles and clustering of low- $z$ galaxies

We have also measured  $w_p(r_p)n$  and  $w_p(r_p)$  for the eight volume limited samples of low-redshift galaxies listed in Table 2 and for different intervals of photometric galaxy luminosity. Since the volume covered by these spectroscopic samples is small due to their small redshift intervals, the  $w_p(r_p)n$  and  $w_p(r_p)$  measurements are more noisy than presented above for the LRG samples. In order to improve the S/N of our measurements, for a given luminosity interval of photometric galaxies we combine the measurements for spectroscopic samples that share a same luminosity interval but span different redshift ranges. When doing the combination we weight each sample by its comoving volume divided by the variance of the measurement, in the same way as above when combining redshift sub-shells. The combined  $w_p(r_p)n$  are plotted in Figure 11. We do not include independent plots for  $w_p(r_p)$ , which show behaviors very similar to  $w_p(r_p)n$ .

In Figure 12 we show the corresponding relative bias factors, based on data points over  $1.9 \leq r_p \leq 10h^{-1}\text{Mpc}$ . Results are plotted in blue, red and green curves for the three luminosity intervals of spectroscopic galaxies. For comparison we also repeat the bias factors from previous work by Tegmark et al. (2004) and Li et al. (2006) which are based on spectroscopic samples similar to those used here. Our measurements are roughly in agreement with these previous determinations. Our bias factors from the three samples agree with each other at the intermediate luminosities around  $L_*$ , while showing obvious deviations at the bright and faint ends. Again, these differences should not be regarded as significant due to large uncertainties.

Similar to what is found for LRGs at  $z \sim 0.4$ , the density profiles around galaxies in the local universe also shows quite similar slope, independent of the luminosity of surrounding photometric galaxies. Unlike in the LRG samples, the spectroscopic galaxies in our low-redshift samples could be either centrals or satellites of their host halos. However, the fraction of satellites should be small as the spectroscopic objects in the SDSS are relatively bright (Zheng et al. 2007). Thus our conclusion made above for  $z \sim 0.4$  more or less holds for the local Universe, that is, satellite galaxies of different luminosities are distributed within their halos in a similar way, if the halos host central galaxies of similar luminosity. This is consistent with previous studies (e.g. Vale & Ostriker 2004, 2006; Zheng et al. 2007) which have revealed a tight relation between central galaxy luminosity  $\langle L_c \rangle$  and halo mass. Moreover, halo occupation distribution models usually assume galaxy distribution inside halos to trace their dark matter, based on studies of satellite distributions in simulations (e.g. Nagai & Kravtsov 2005; Macciò et al. 2006). Again, our results provide additional, clear evidence for supporting this assumption.

### 5. Discussion and Summary

Previous studies on galaxy clustering as a function of luminosity usually make use of spectroscopic galaxy catalogue, thus are limited to relatively bright galaxies and low redshifts. In this work we have developed a new method which measures simultaneously the projected number

density profile  $w_p(r_p)n$  and the projected cross-correlation function  $w_p(r_p)$  of a set of photometric galaxies, surrounding a set of spectroscopic galaxies. We are able to divide the photometric galaxies by luminosity even when redshift information is unavailable. This enables us to measure  $w_p(r_p)n$  and  $w_p(r_p)$  as a function of not only the luminosity of the spectroscopic galaxies, but also that of the surrounding photometric galaxies. Since photometric samples are usually much larger and fainter than spectroscopic ones, with our method one can explore the clustering of galaxies to fainter luminosities at high redshift.

We have applied our method to the SDSS data including a sample of  $10^5$  luminous red galaxy (LRGs) at  $z \sim 0.4$  and a sample of about half a million galaxies at  $z \sim 0.1$ . Both are cross-correlated with an SDSS photometric sample consisting of about 20 million galaxies down to  $r = 21$ . We have investigated the dependence of  $w_p(r_p)n$  and  $w_p(r_p)$  on galaxy luminosity and redshift, by dividing both spectroscopic and photometric galaxies into various luminosity intervals and different redshift ranges.

The conclusions of this paper can be summarized as follows.

- We develop a new method which measures the projected density distribution  $w_p(r_p)n$  of photometric galaxies surrounding a set of spectroscopically-identified galaxies, and simultaneously the projected cross-correlation function  $w_p(r_p)$  between the two populations. In this method we are able to divide the photometric galaxies into subsamples in luminosity intervals even when redshift information is unavailable, enabling us to measure  $w_p(r_p)n$  and  $w_p(r_p)$  as a function of not only the luminosity of the spectroscopic galaxy, but also that of the photometric galaxy. Extensive tests show that our method can measure  $w_p(r_p)$  in a statistically unbiased way. The accuracy of the measurement depends on the validity of the assumption inherent to the method that the foreground/background galaxies are randomly distributed and are thus uncorrelated with those galaxies of interest. Therefore, our method can be applied to the cases where foreground/background galaxies are distributed in large volumes, which is usually valid in real observations.
- We find that, for a spectroscopic sample at given luminosity and redshift, the projected cross-correlation function and projected density profile as traced by photometric galaxies show quite similar slope to each other, independent of the luminosity of the photometric galaxies. This indicates that satellite galaxies of different luminosities are distributed in a similar way within their host dark matter halos. This is true not only for LRGs at intermediate redshifts which are mostly central galaxies of their halos, but also for the general population of galaxies in the local Universe. Our result provides observational support for the assumption commonly-adopted in halo occupation distribution models that the distribution of galaxies follows the dark matter distribution within their halos.
- The relative bias factors are estimated for photometric galaxies as a function of luminosity and redshift. In particular, we measured the bias factors of such kind, for the first time, for galaxies at intermediate redshift ( $z \sim 0.4$ ) over a wide range in luminosity ( $0.3L_* < L < 5L_*$ ).

There have been previous studies of measuring galaxy clustering by cross-correlations with imaging data. Although the methods and purposes of these studies are different from ours, it is worthy of mentioning them and pointing out the findings in common. Eisenstein et al. (2005) measured the mean overdensity around LRGs in an earlier SDSS release by cross-correlating 32,000 LRGs with 16 million photometric galaxies, using the deprojecting method developed in (Eisenstein 2003). The authors were aimed at understanding the scale- and luminosity-dependence of the clustering of LRGs, thus using only  $L_*$  galaxies from the photometric sample as a tracer of the surrounding distribution. In our work we consider luminosity dependence for both LRGs and photometric galaxies, and this is why we have made considerable efforts on selecting photometric galaxies of specific luminosities. Our measurements from cross-correlation with  $L_*$  galaxies show strong dependence in  $w_p(r_p)$  amplitude on LRG luminosity, as well as an obvious transition at around 1 Mpc/ $h$ , which are in agreement with what those authors find.

Masjedi et al. (2006) measured the cross-correlation between  $\sim 25,000$  LRGs and an imaging sample, in order to correct for the effect of fiber collisions on their small-scale measurements of LRG auto-correlations. They find that the real-space auto-correlation function of LRGs,  $\xi(r)$ , is surprisingly close to a  $r^{-2}$  power law over more than 4 orders of magnitude in separation  $r$ , down to  $r \sim 15$  kpc/ $h$ . We don't have a measurement of auto-correlations  $\xi(r)$  or  $w_p(r_p)$  for LRGs, but our results are not inconsistent with theirs in the sense that the projected cross-correlation of our LRG samples continuously increases at such small scales, with a slope similar to that on large scales. In a recent work, White et al. (2011) studied the clustering of massive galaxies at  $z \sim 0.5$  using the first semester of BOSS data. The authors computed the projected cross-correlation between their imaging catalogue and the spectroscopic one, as an additional analysis to emphasize that there is a significant power on scales below 0.3 Mpc/ $h$  where their spectroscopy-based measurements suffer from fiber collisions. This is obviously consistent with what we have seen from our measurements.

Our method can be applied and extended to many important statistical studies of galaxy formation and evolution. By dividing galaxies into red and blue populations in the photometric sample according to their colors, we can quantify the evolution of the blue fraction of galaxies in clusters and groups from redshift 0.4 to the present day (i.e the Butcher-Oemler effect, e.g. Goto et al. 2003; De Propris et al. 2004). Wide deep photometry surveys, such as Pan-Starrs (Kaiser 2004) and LSST (Tyson 2002), will be available in the next years. Combining such surveys with large spectroscopic samples, such as BOSS LRG samples, will allow one to explore the clustering of galaxies from  $z = 0$  up to  $z = 1$  for a wide range of luminosities. The WISE (Wright et al. 2010) will produce an all-sky catalogue of infrared galaxies. By combining this survey with SDSS spectroscopic samples, one can study how infrared galaxies are distributed relative to the network of optical galaxies.

This work is supported by NSFC (10821302, 10878001), by the Knowledge Innovation Program of CAS (No. KJCX2-YW-T05), by 973 Program (No. 2007CB815402), and by the CAS/SAFEA International Partnership Program for Creative Research Teams (KJCX2-YW-T23).

## REFERENCES

- Abazajian, K. N., et al. 2009, *ApJS*, 182, 543
- Bardeen, J. M., Bond, J. R., Kaiser, N., & Szalay, A. S. 1986, *ApJ*, 304, 15
- Benson, A. J., Baugh, C. M., Cole, S., Frenk, C. S., & Lacey, C. G. 2000, *MNRAS*, 316, 107
- Berlind, A. A., & Weinberg, D. H. 2002, *ApJ*, 575, 587
- Blanton, M. R., et al. 2003, *ApJ*, 592, 819
- Blanton, M. R., Lin, H., Lupton, R. H., Maley, F. M., Young, N., Zehavi, I., & Loveday, J. 2003, *AJ*, 125, 2276
- Blanton, M. R., et al. 2005, *AJ*, 129, 2562
- Blanton, M. R., & Roweis, S. 2007, *AJ*, 133, 734
- Carlberg, R. G., Yee, H. K. C., Morris, S. L., Lin, H., Hall, P. B., Patton, D. R., Sawicki, M., & Shepherd, C. W. 2001, *ApJ*, 563, 736
- Chen, J., Kravtsov, A. V., Prada, F., Sheldon, E. S., Klypin, A. A., Blanton, M. R., Brinkmann, J., & Thakar, A. R. 2006, *ApJ*, 647, 86
- Coil, A. L., et al. 2004, *ApJ*, 609, 525
- Coil, A. L., Newman, J. A., Cooper, M. C., Davis, M., Faber, S. M., Koo, D. C., & Willmer, C. N. A. 2006, *ApJ*, 644, 671
- Coil, A. L., et al. 2008, *ApJ*, 672, 153
- Colberg, J. M., et al. 2000, *MNRAS*, 319, 209
- Colless, M., et al. 2001, *MNRAS*, 328, 1039
- Cooray, A., & Sheth, R. 2002, *Phys. Rep.*, 372, 1
- Davis, M., & Peebles, P. J. E. 1983, *ApJ*, 267, 465
- Davis, M., Efstathiou, G., Frenk, C. S., & White, S. D. M. 1985, *ApJ*, 292, 371
- Davis, M., et al. 2003, *Proc. SPIE*, 4834, 161
- de la Torre, S., et al. 2009, *arXiv:0911.2252*
- De Propris, R., et al. 2004, *MNRAS*, 351, 125
- Eisenstein, D. J., et al. 2001, *AJ*, 122, 2267

- Eisenstein, D. J. 2003, *ApJ*, 586, 718
- Eisenstein, D. J., Blanton, M., Zehavi, I., Bahcall, N., Brinkmann, J., Loveday, J., Meiksin, A., & Schneider, D. 2005, *ApJ*, 619, 178
- Faber, S. M., et al. 2007, *ApJ*, 665, 265
- Firth, A. E., et al. 2002, *MNRAS*, 332, 617
- Goto, T., Yamauchi, C., Fujita, Y., Okamura, S., Sekiguchi, M., Smail, I., Bernardi, M., & Gomez, P. L. 2003, *MNRAS*, 346, 601
- Goto, T., et al. 2003, *PASJ*, 55, 739
- Guo, Q., White, S., Li, C., & Boylan-Kolchin, M. 2010, *MNRAS*, 404, 1111
- Hamilton, A. J. S. 1993, *ApJ*, 417, 19
- Hamilton, A. J. S., & Tegmark, M. 2002, *MNRAS*, 330, 506
- Jing, Y. P. 1998, *ApJ*, 503, L9
- Jing, Y. P., Mo, H. J., & Boerner, G. 1998, *ApJ*, 494, 1
- Jing, Y. P., & Boerner, G. 1998, *ApJ*, 503, 37
- Kaiser, N. 1984, *ApJ*, 284, L9
- Kaiser, N. 2004, *Proc. SPIE*, 5489, 11
- Kauffmann, G., Nusser, A., & Steinmetz, M. 1997, *MNRAS*, 286, 795
- Kauffmann, G., Colberg, J. M., Diaferio, A., & White, S. D. M. 1999, *MNRAS*, 303, 188
- Kazin, E. A., et al. 2010, *ApJ*, 710, 1444
- Larson, D., et al. 2010, *arXiv:1001.4635*
- Lake, G., & Tremaine, S. 1980, *ApJ*, 238, L13
- Le Fèvre, O., et al. 2005, *A&A*, 439, 845
- Li, C., Kauffmann, G., Jing, Y. P., White, S. D. M., Börner, G., & Cheng, F. Z. 2006, *MNRAS*, 368, 21
- Li, C., Jing, Y. P., Kauffmann, G., Börner, G., Kang, X., & Wang, L. 2007, *MNRAS*, 376, 984
- Lilly, S. J., et al. 2007, *ApJS*, 172, 70

- Lorrimer, S. J., Frenk, C. S., Smith, R. M., White, S. D. M., & Zaritsky, D. 1994, MNRAS, 269, 696
- Ma, C.-P., & Fry, J. N. 2000, ApJ, 543, 503
- Macciò, A. V., Moore, B., Stadel, J., & Diemand, J. 2006, MNRAS, 366, 1529
- Madgwick, D. S., et al. 2003, MNRAS, 344, 847
- Masjedi, M., et al. 2006, ApJ, 644, 54
- Meneux, B., et al. 2006, A&A, 452, 387
- Meneux, B., et al. 2008, A&A, 478, 299
- Meneux, B., et al. 2009, A&A, 505, 463
- Mo, H. J., & White, S. D. M. 1996, MNRAS, 282, 347
- Nagai, D., & Kravtsov, A. V. 2005, ApJ, 618, 557
- Navarro, J. F., Frenk, C. S., & White, S. D. M. 1997, ApJ, 490, 493
- Norberg, P., et al. 2002, MNRAS, 332, 827
- Norberg, P., et al. 2001, MNRAS, 328, 64
- Okumura, T., Jing, Y. P., & Li, C. 2009, ApJ, 694, 214
- Peacock, J. A., & Dodds, S. J. 1996, MNRAS, 280, L19
- Peacock, J. A., & Smith, R. E. 2000, MNRAS, 318, 1144
- Phillipps, S., & Shanks, T. 1987, MNRAS, 229, 621
- Phleps, S., Peacock, J. A., Meisenheimer, K., & Wolf, C. 2006, A&A, 457, 145
- Reid, B. A., & Spergel, D. N. 2009, ApJ, 698, 143
- Ross, A. J., Brunner, R. J., & Myers, A. D. 2007, ApJ, 665, 67
- Sales, L., & Lambas, D. G. 2005, MNRAS, 356, 1045
- Schechter, P. 1976, ApJ, 203, 297
- Scoccimarro, R., Sheth, R. K., Hui, L., & Jain, B. 2001, ApJ, 546, 20
- Seljak, U., & Zaldarriaga, M. 1996, ApJ, 469, 437
- Seljak, U. 2000, MNRAS, 318, 203

- Seljak, U., & Warren, M. S. 2004, MNRAS, 355, 129
- Shepherd, C. W., Carlberg, R. G., Yee, H. K. C., Morris, S. L., Lin, H., Sawicki, M., Hall, P. B., & Patton, D. R. 2001, ApJ, 560, 72
- Sheth, R. K., & Tormen, G. 1999, MNRAS, 308, 119
- Tegmark, M., Hamilton, A. J. S., & Xu, Y. 2002, MNRAS, 335, 887
- Tegmark, M., et al. 2004, ApJ, 606, 702
- Tinker, J. L., Weinberg, D. H., Zheng, Z., & Zehavi, I. 2005, ApJ, 631, 41
- Tyson, J. A. 2002, Proc. SPIE, 4836, 10
- Vader, J. P., & Sandage, A. 1991, ApJ, 379, L1
- Vale, A., & Ostriker, J. P. 2006, MNRAS, 371, 1173
- Vale, A., & Ostriker, J. P. 2004, MNRAS, 353, 189
- Wang, L., & Jing, Y. P. 2010, MNRAS, 402, 1796
- Westra, E., Geller, M. J., Kurtz, M. J., Fabricant, D. G., Dell’Antonio, I., Astrophysical Observatory, S., & University, B. 2010, arXiv:1006.2823
- White, M., et al. 2010, arXiv:1010.4915
- White, S. D. M., & Rees, M. J. 1978, MNRAS, 183, 341
- White, S. D. M., & Frenk, C. S. 1991, ApJ, 379, 52
- White, M., et al. 2011, ApJ, 728, 126
- Wright, E. L., et al. 2010, AJ, 140, 1868
- Yang, X., Mo, H. J., & van den Bosch, F. C. 2003, MNRAS, 339, 1057
- York, D. G., et al. 2000, AJ, 120, 1579
- Zaldarriaga, M., & Seljak, U. 2000, ApJS, 129, 431
- Zaldarriaga, M., Seljak, U., & Bertschinger, E. 1998, ApJ, 494, 491
- Zehavi, I., et al. 2002, ApJ, 571, 172
- Zehavi, I., et al. 2005, ApJ, 621, 22
- Zehavi, I., et al. 2005, ApJ, 630, 1

Zehavi, I., et al. 2010, arXiv:1005.2413

Zhao, D. H., Jing, Y. P., Mo, H. J., Börner, G. 2009, ApJ, 707, 354

Zheng, Z., et al. 2005, ApJ, 633, 791

Zheng, Z., Coil, A. L., & Zehavi, I. 2007, ApJ, 667, 760



Table 1. LRG samples selected according to luminosity and redshift

SAMPLE (1)	$M_{0.3g}$ (2)	$z$ (3)	Num. of galaxies (4)	Sub-shell information	
				Num. of sub-shells (5)	$\Delta z_{sub}$ (6)
L1	(-23.2,-21.8)	(0.16,0.26)	5592	5	0.02
L2	(-21.8,-21.2)	(0.16,0.26)	16832	5	0.02
L3	(-23.2,-21.8)	(0.26,0.36)	11647	5	0.02
L4	(-21.8,-21.2)	(0.26,0.36)	26301	5	0.02
L5	(-23.2,-21.8)	(0.36,0.46)	17502	5	0.02

Table 2. Low-redshift volume-limited samples of galaxies selected by luminosity and redshift

SAMPLE (1)	$M_{0.1r}$ (2)	$z$ (3)	Num. of galaxies (4)	Sub-shell information	
				Num. of sub-shells (5)	$\Delta z_{sub}$ (6)
VL1	(-21.0,-20.2)	(0.03,0.07)	20553	10	0.004
VL2	(-23.0,-21.0)	(0.03,0.07)	5879	10	0.004
VL3	(-21.0 -20.2)	(0.07,0.11)	63694	5	0.008
VL4	(-23.0 -21.0)	(0.07,0.11)	19138	5	0.008
VL5	(-23.0,-21.0)	(0.11,0.15)	40226	4	0.01
VL6	(-23.0,-21.9)	(0.11,0.15)	2330	4	0.01
VL7	(-23.0,-21.9)	(0.15,0.19)	3935	4	0.01
VL8	(-23.0,-21.9)	(0.19,0.23)	5268	4	0.01

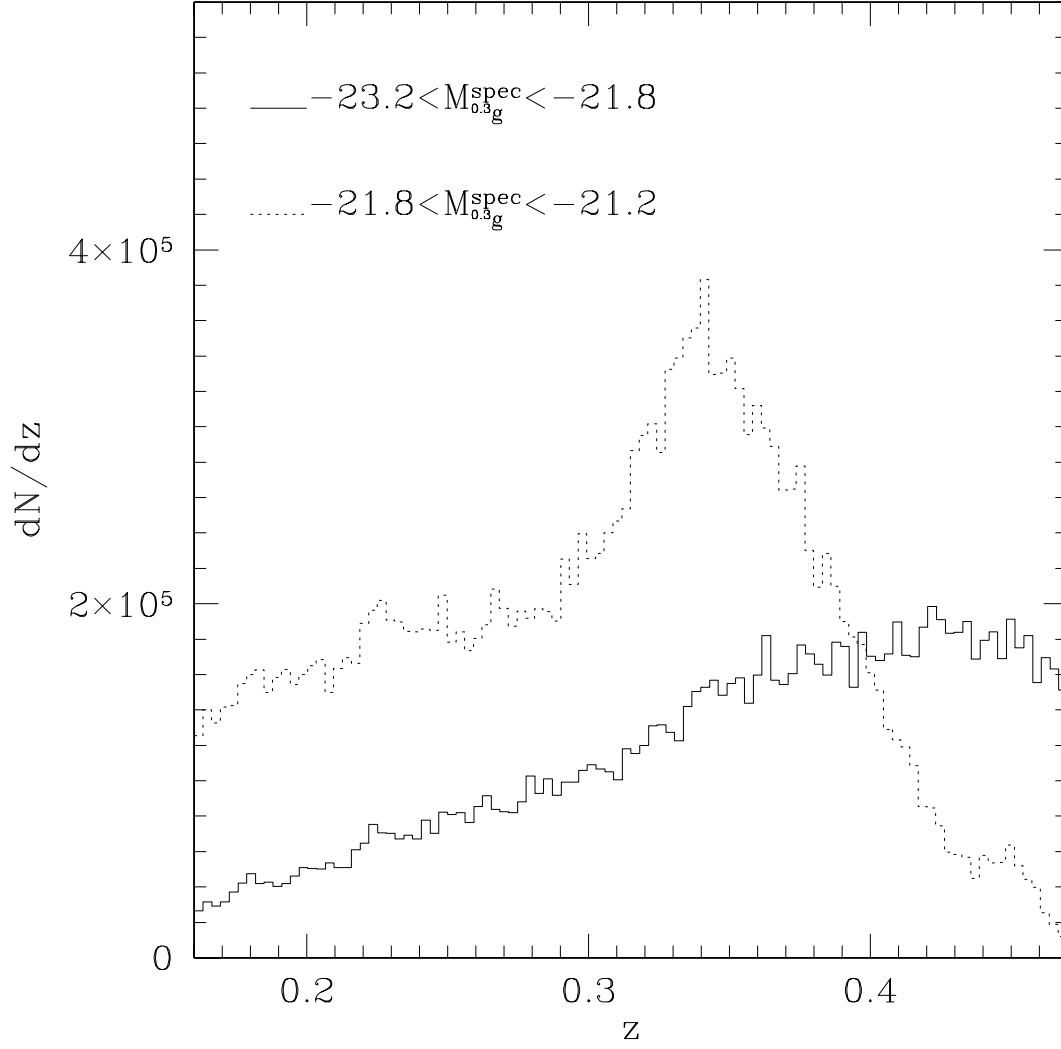


Fig. 1.— Redshift histograms for luminous red galaxies (LRGs) in our sample falling in the two luminosity intervals, as indicated, which we use to select our subsamples in Table 1. The g-band absolute magnitude  $M_{0.3g}$  is  $K$ - and  $E$ - corrected to its value at  $z = 0.3$ .

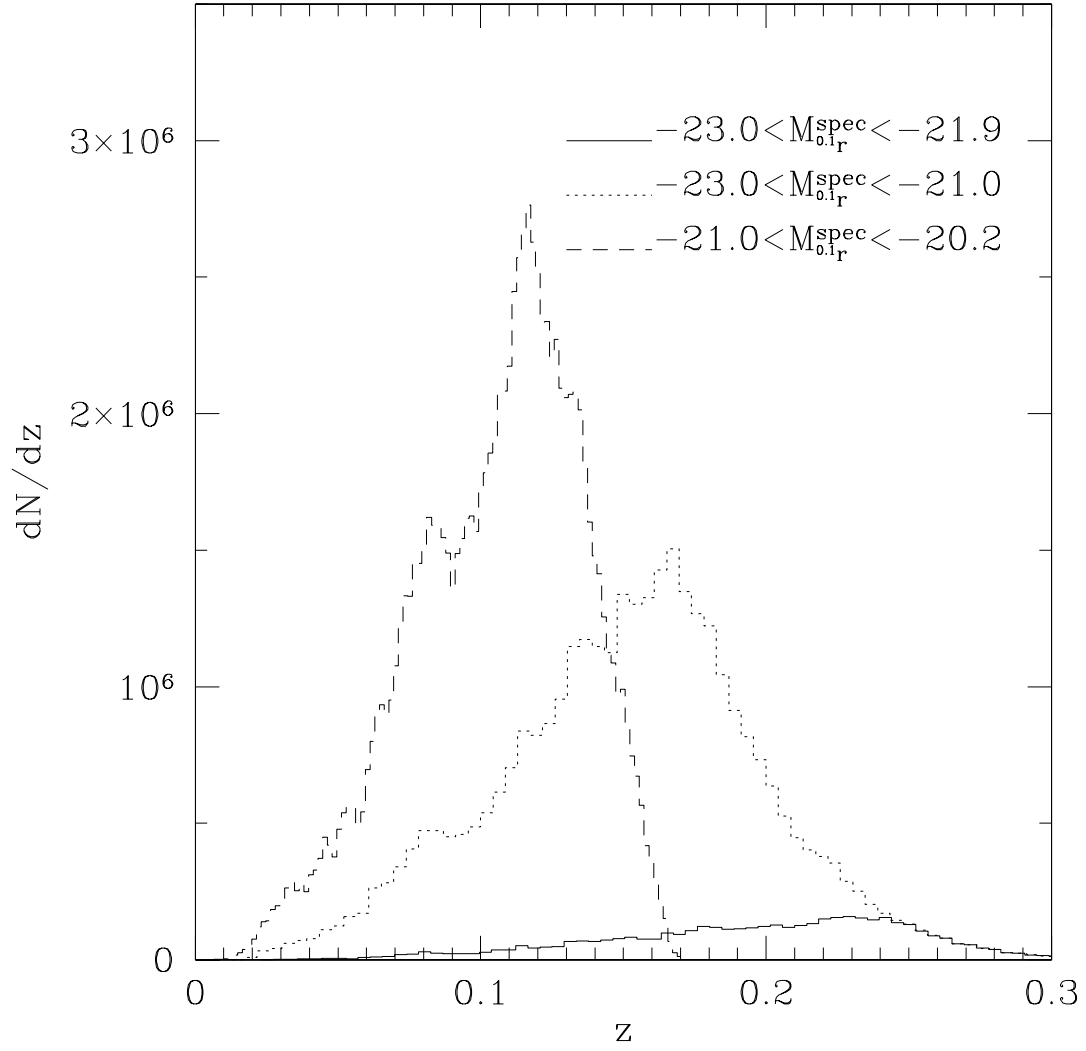


Fig. 2.— Redshift histograms for spectroscopic galaxies in our low-redshift sample in three different luminosity ranges as indicated, which we use to select our subsamples in Table 2. The  $r$ -band absolute magnitude  $M_{0.1g}$  is  $K$ - and  $E$ - corrected to its value at  $z = 0.1$ .

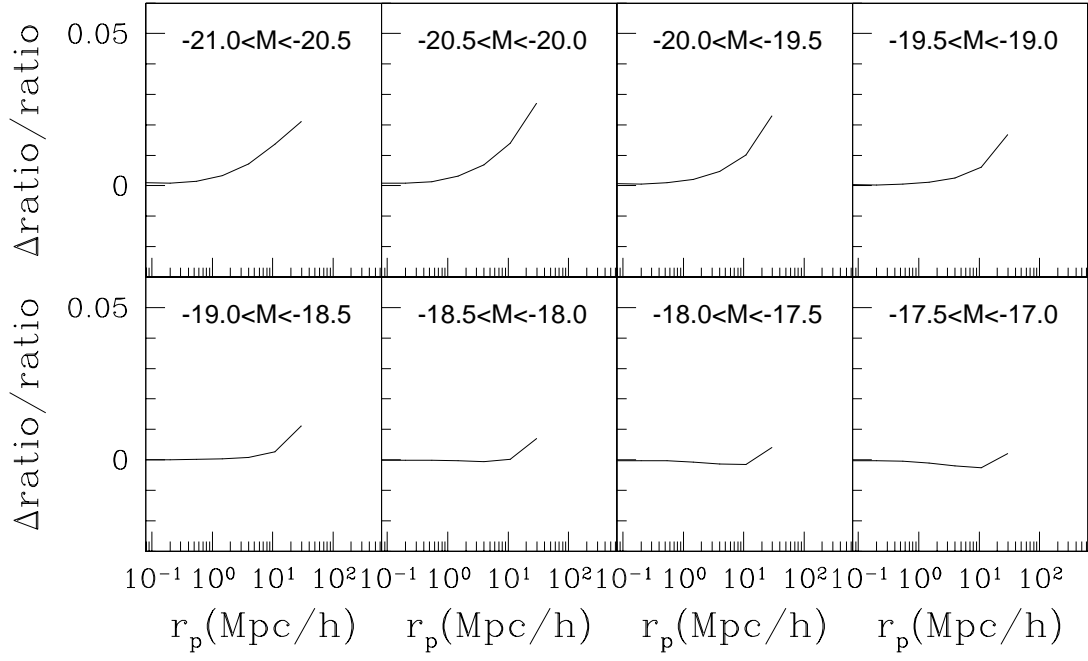


Fig. 3.— Relative difference in  $w(\theta)/w_p(r_p)$  ratio between the value from Eqn. (13) and the value from theoretical calculation (see § 3.3.1 for details), for spectroscopic galaxies at  $0.07 < z < 0.078$  and photometric galaxies at different luminosities, as indicated in each panel.

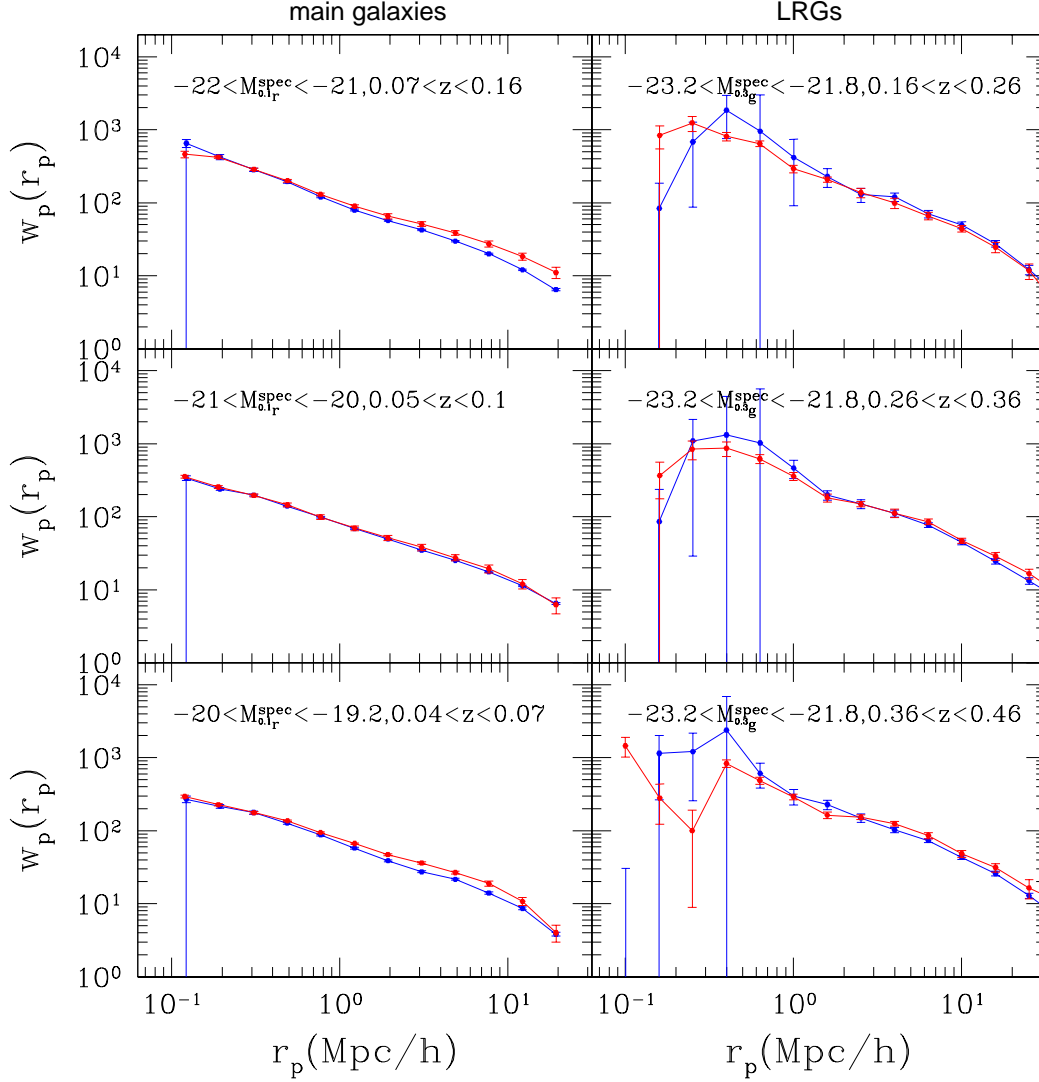


Fig. 4.— Plotted in each panel (red symbols connected by a red line) is  $w_p(r_p)$  of spectroscopic galaxies at given luminosity and redshift ranges (as indicated), estimated from cross-correlation with photometric galaxies in the same luminosity and redshift ranges. This is compared to the projected auto-correlation correlation function of the same set of spectroscopic galaxies, as plotted in blue symbols/lines. Panels in the left-hand columns are for galaxies in the low-redshift sample and those in the right are for LRGs.

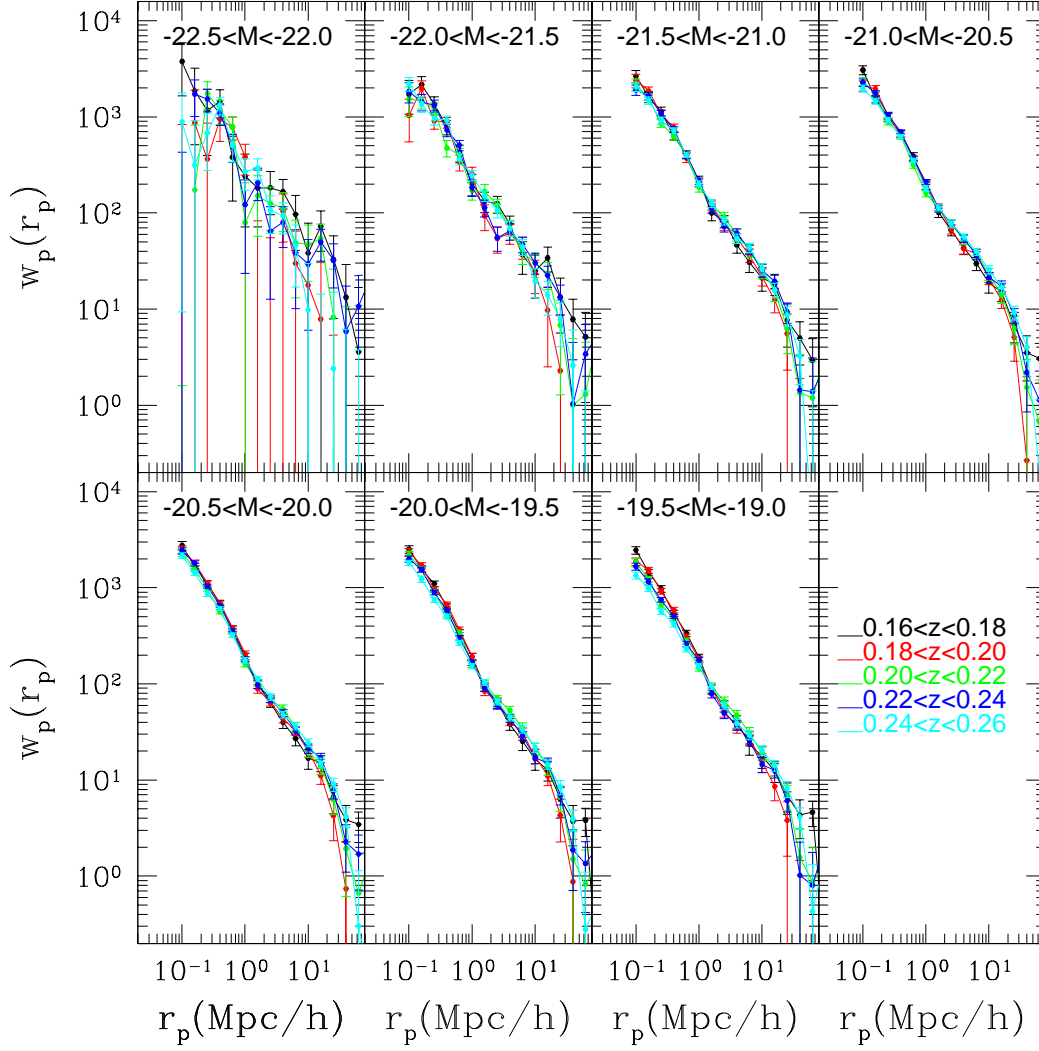


Fig. 5.— Projected cross-correlation function  $w_p(r_p)$  for redshift sub-shells of Sample L1 in Table 1, estimated by cross correlating each sub-shell with photometric galaxies in different luminosity intervals as indicated in each panel. Different lines are for different sub-shells with their redshift ranges indicated in the bottom-right panel.

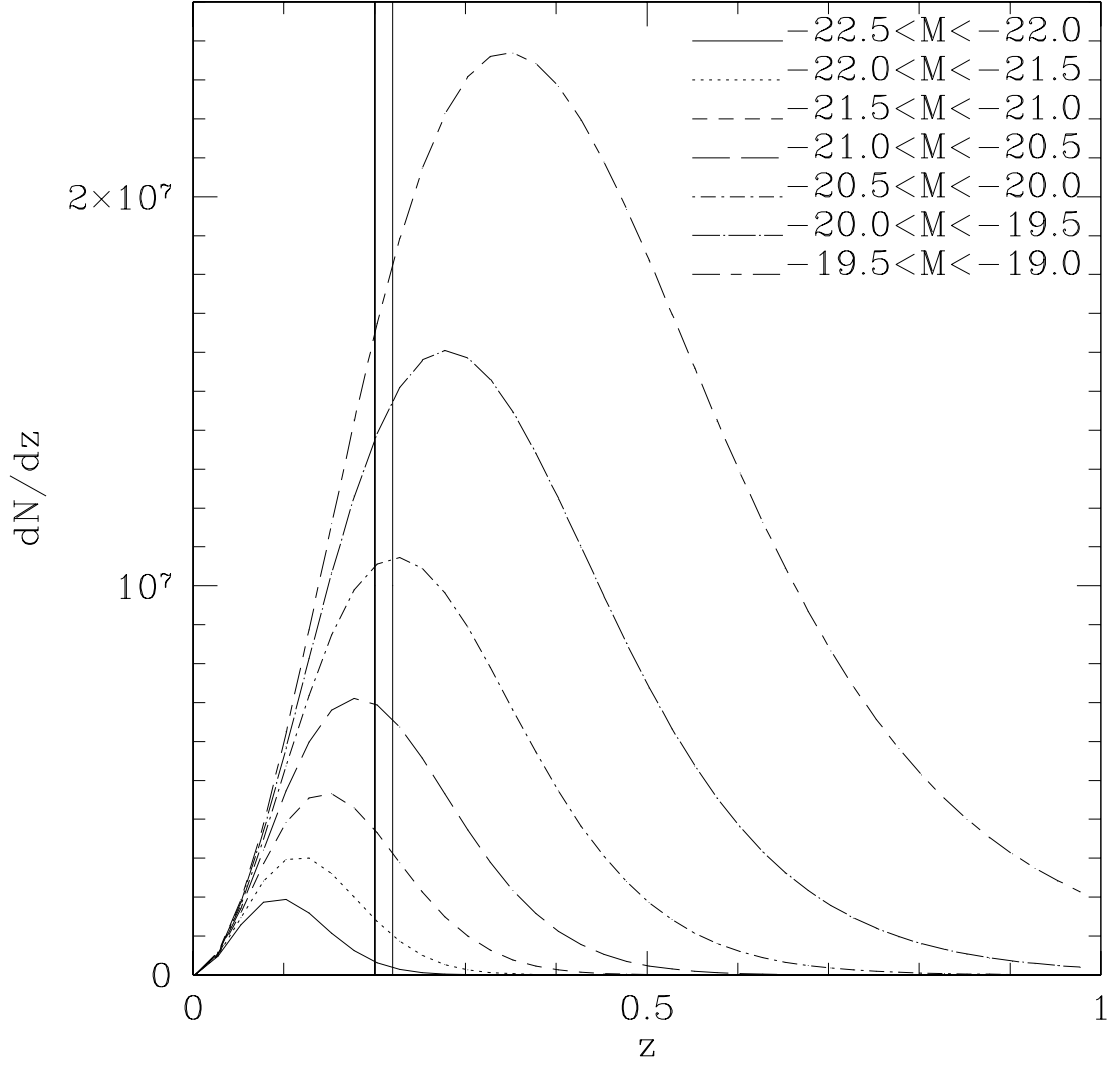


Fig. 6.— Redshift distribution as predicted by the luminosity function from Blanton et al. (2003) for photometric galaxies that are expected to fall in the indicated luminosity intervals if they were located in the redshift range  $0.2 < z < 0.22$ . The two vertical lines mark the redshift range.

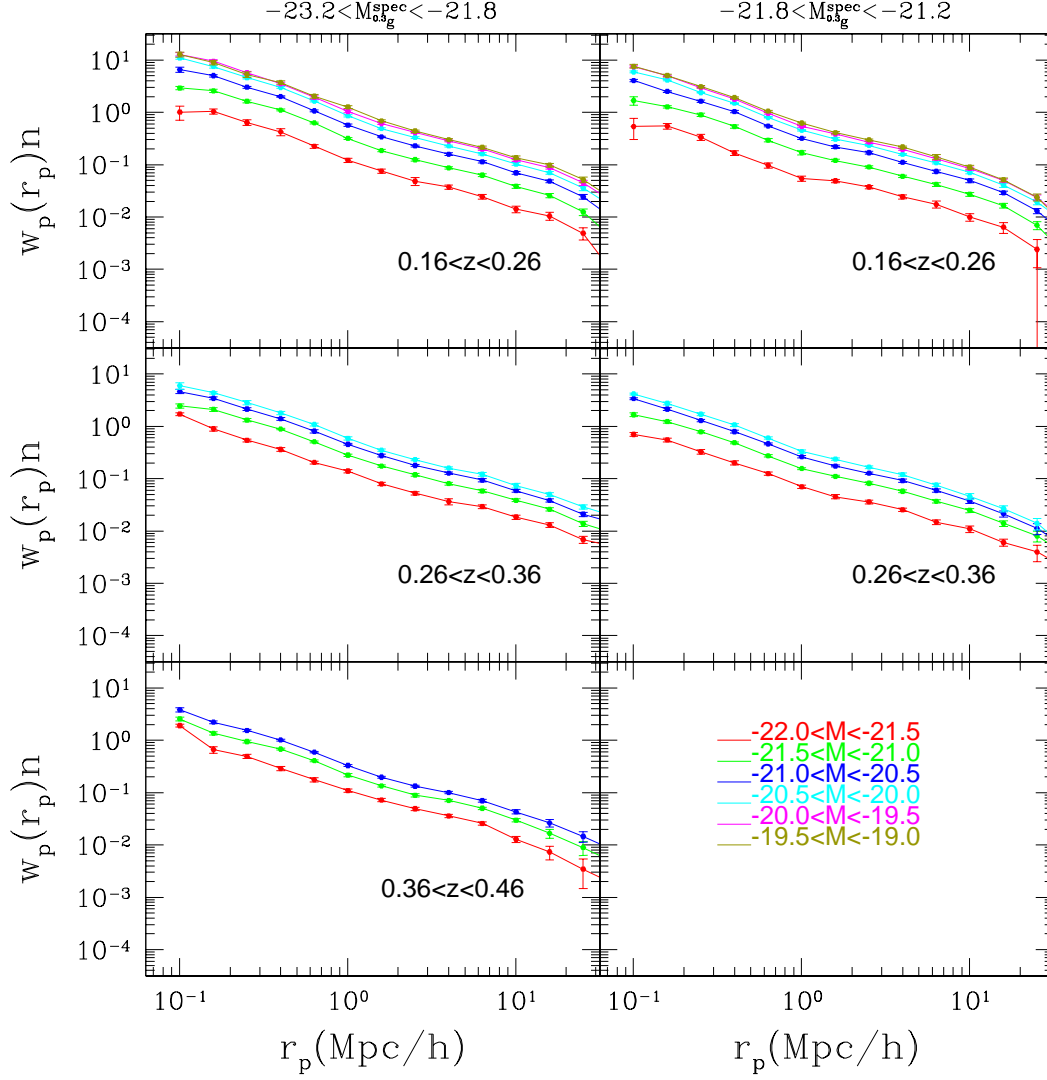


Fig. 7.— Projected density profile  $w_p(r_p)n$  in units of  $Mpc^{-2}h^2$  surrounding LRGs with different luminosities (indicated above the figure) and redshifts (indicated in each panel), as traced by galaxies of different luminosities (shown in different lines in each panel and indicated in the bottom-right panel).



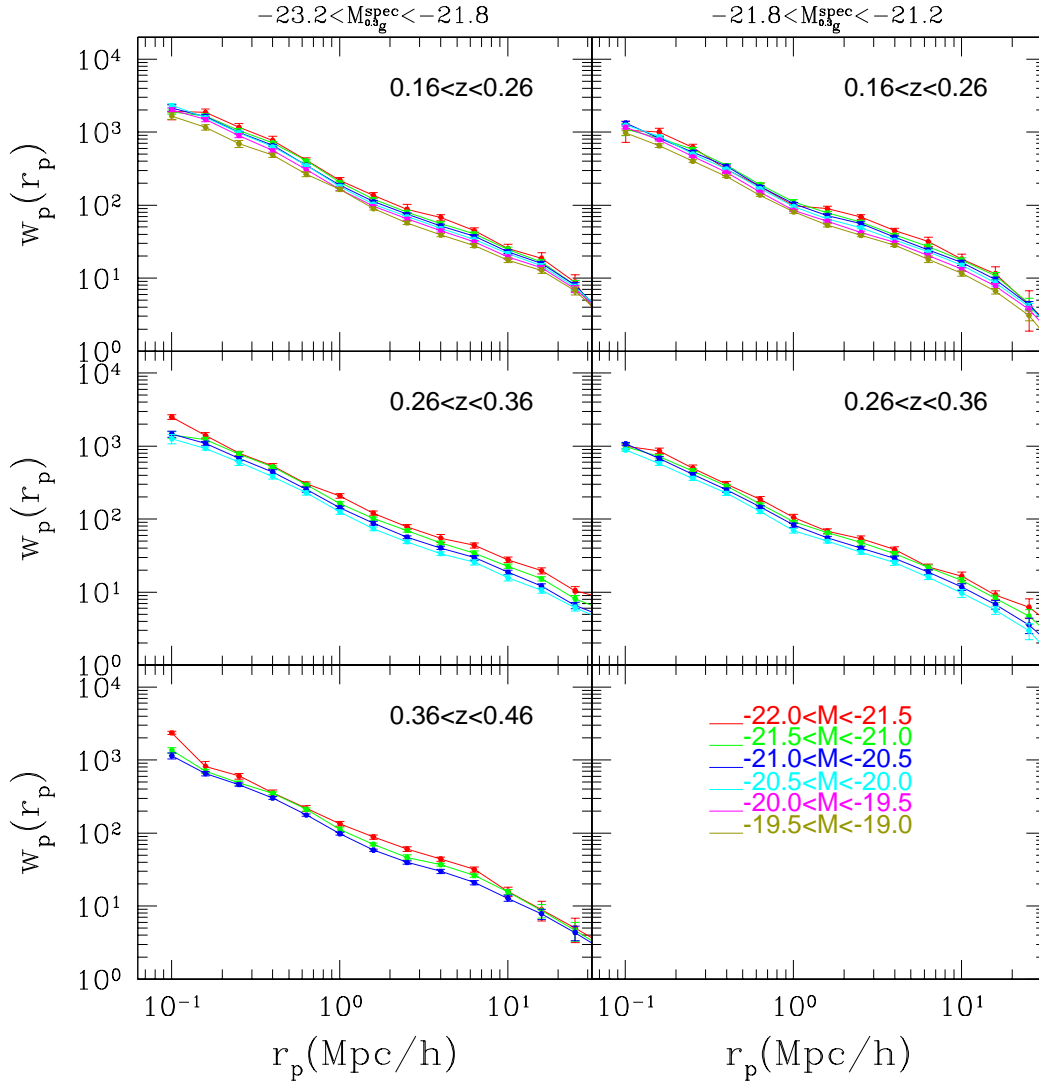


Fig. 8.— Projected cross-correlation function  $w_p(r_p)$  measured for the same set of LRG samples and the same intervals of photometric galaxy luminosity as in the previous figure.

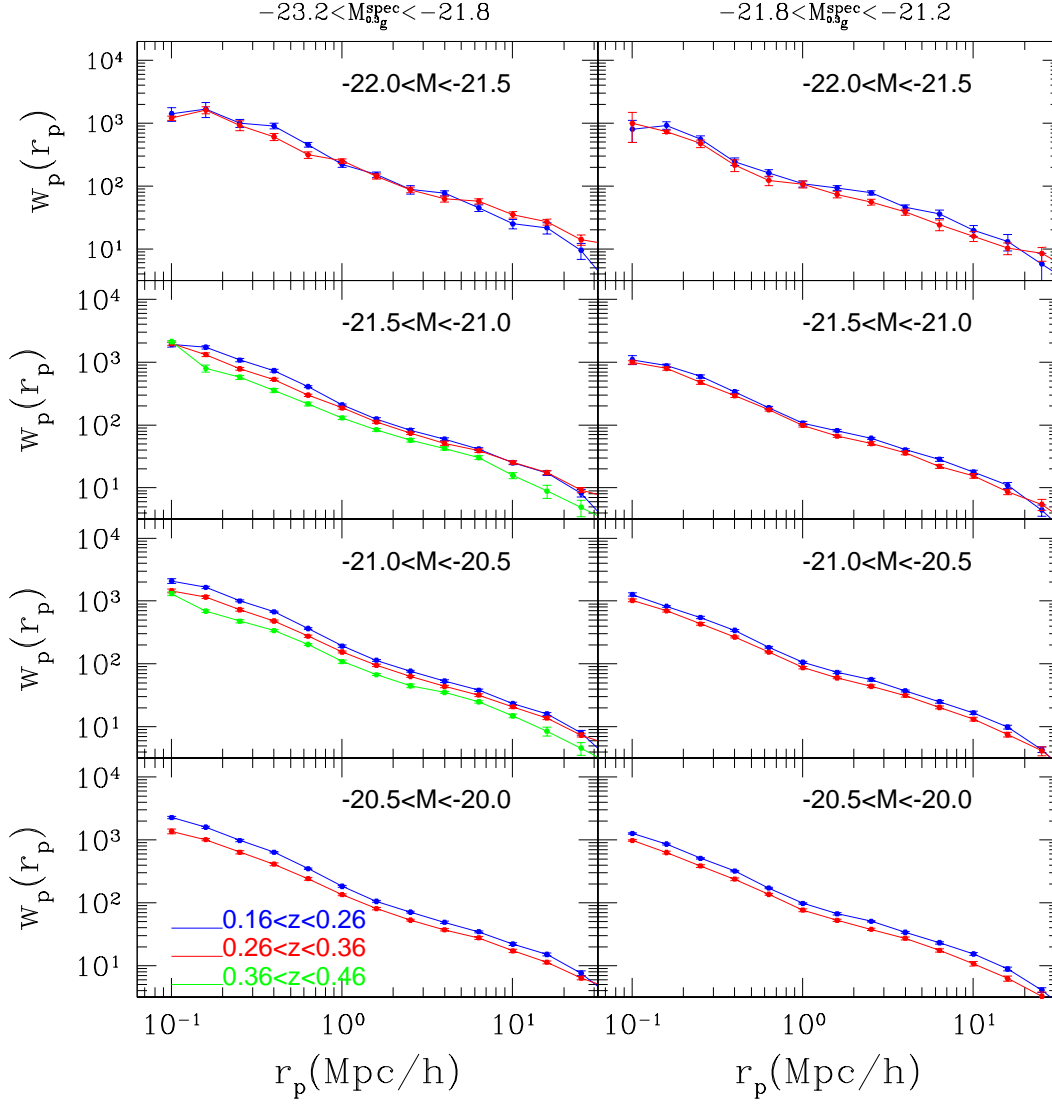


Fig. 9.— Each panel compares  $w_p(r_p)$  measured at different redshifts (as indicated), but for fixed luminosity ranges for photometric and spectroscopic galaxies. The luminosity ranges of spectroscopic galaxies are indicated above the figure, while those of photometric galaxies are indicated in each panel.

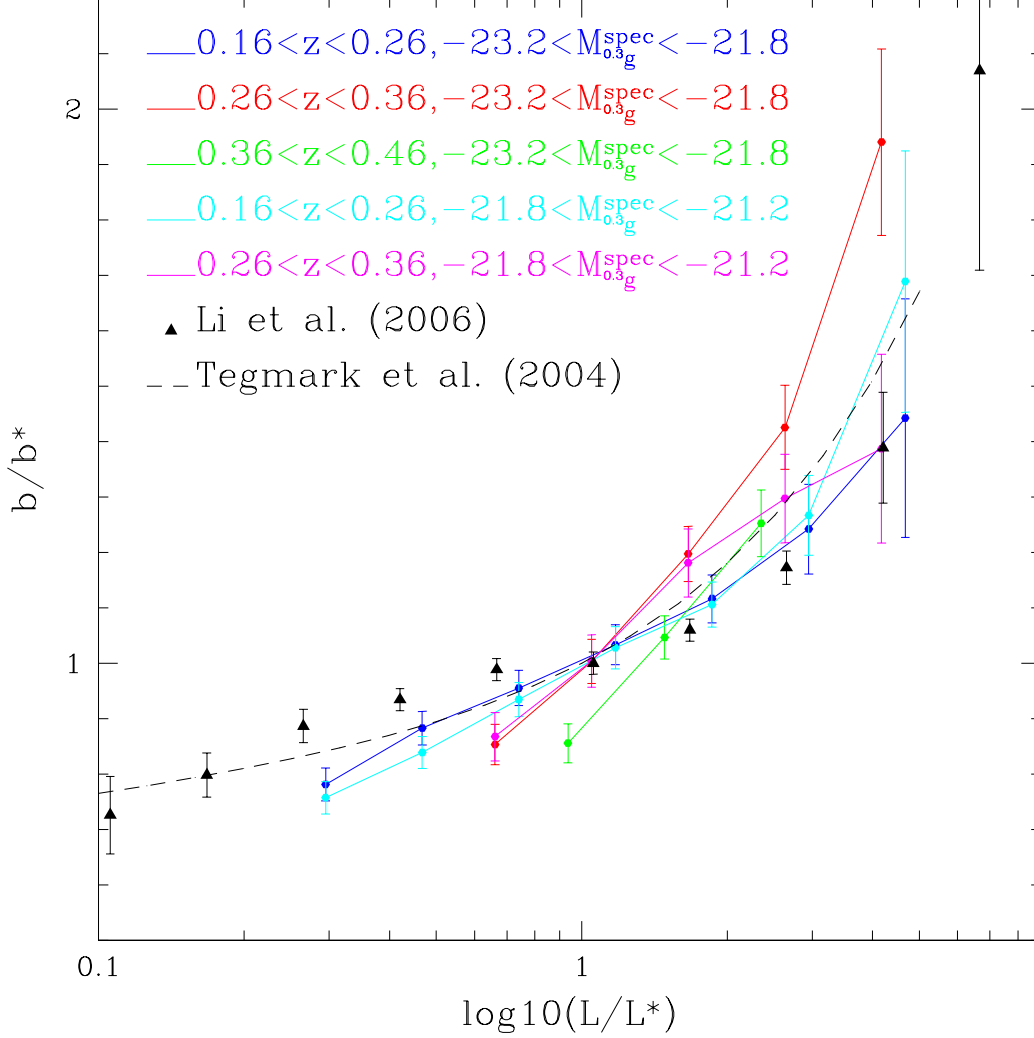


Fig. 10.— Relative bias factor with respect to  $L^*$  as a function of luminosity. Bias factors are calculated from the amplitude of  $w_p(r_p)$  averaged over  $2.5h^{-1}Mpc < r < 10.0h^{-1}Mpc$ , and normalized by  $w_p(r_p)$  between the same LRG sample and the photometric sample with  $-21 < M_{0.1r} < -20$ . Note that for the  $0.36 < z < 0.46$  bin, the photometric catalogue becomes incomplete when  $M > -20.5$ , and so we calculate the relative bias factor with respect to the photometric sample of  $-21.0 < M_{0.1r} < -20.5$ . Different curves are for results obtained with different LRG subsamples, as indicated. Black triangles and the black dashed line show previous determinations from Li et al. (2006) and (Tegmark et al. 2004), which are based on auto-correlation function or power spectrum of the SDSS Main galaxy sample with a mean redshift of  $z \sim 0.1$ .

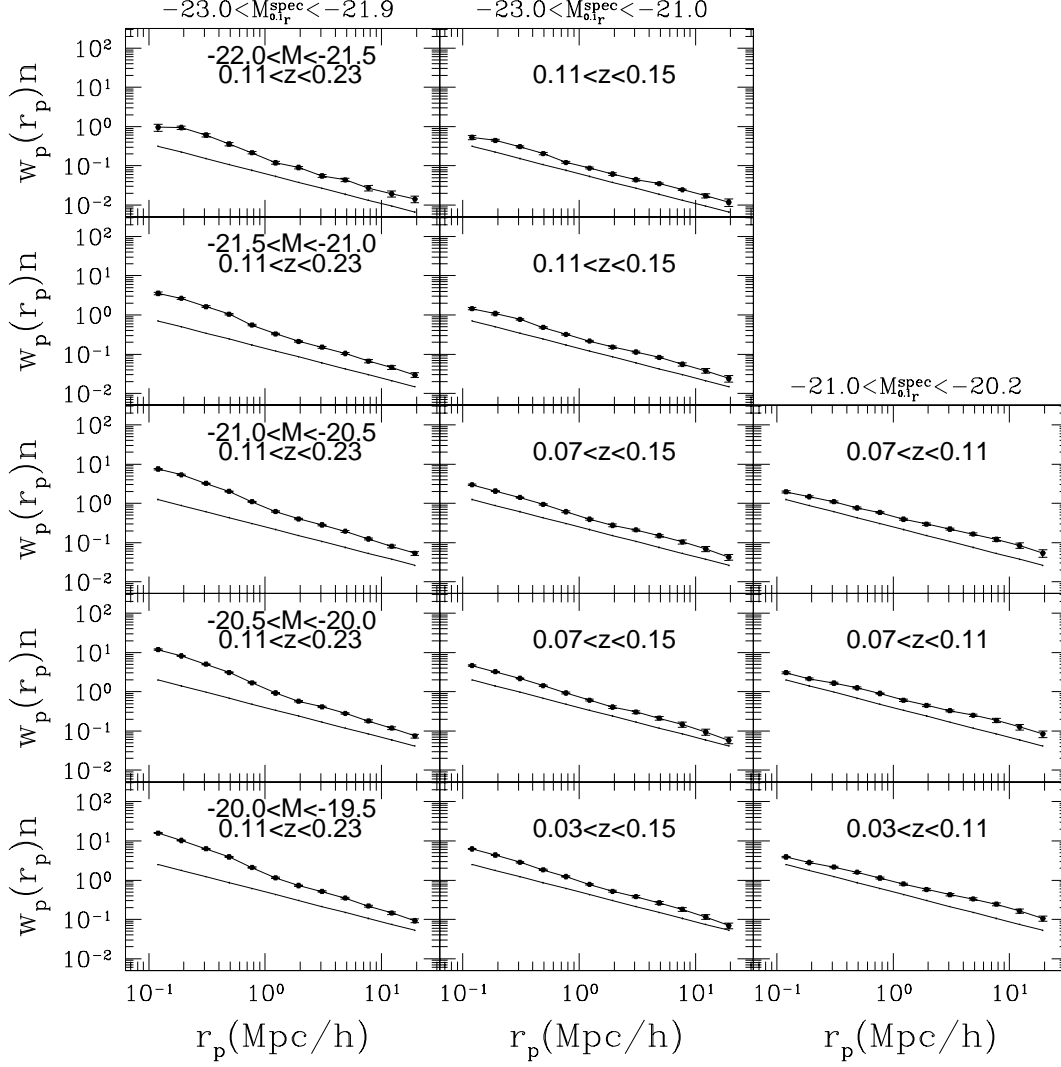


Fig. 11.— Projected cross-correlation function  $w_p(r_p)$  between spectroscopic galaxies of different luminosities (indicated above each column) and photometric galaxies of different luminosities and redshifts (both indicated in each panel). A solid black line is repeated on every panel to guide the eye.

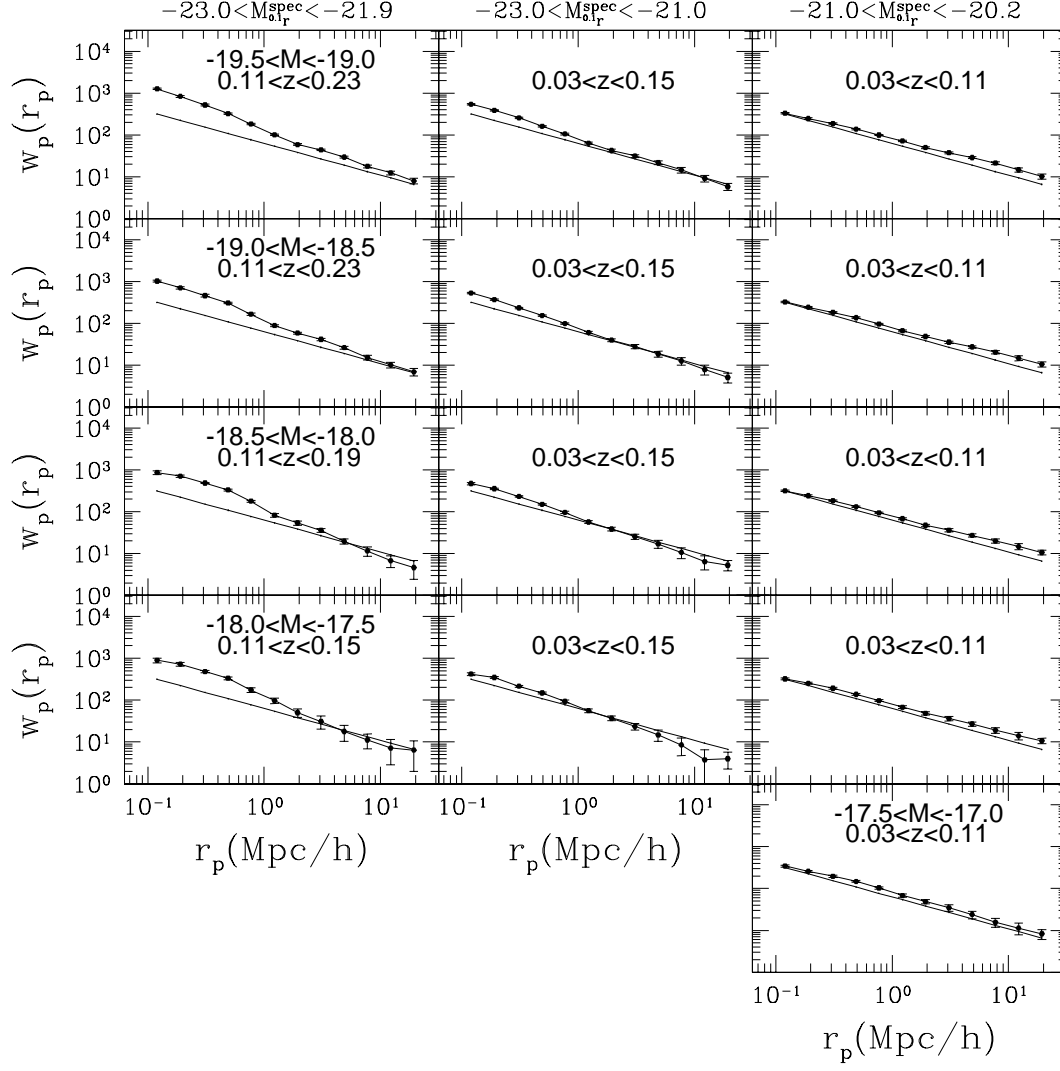


Fig. 11.— Continued...

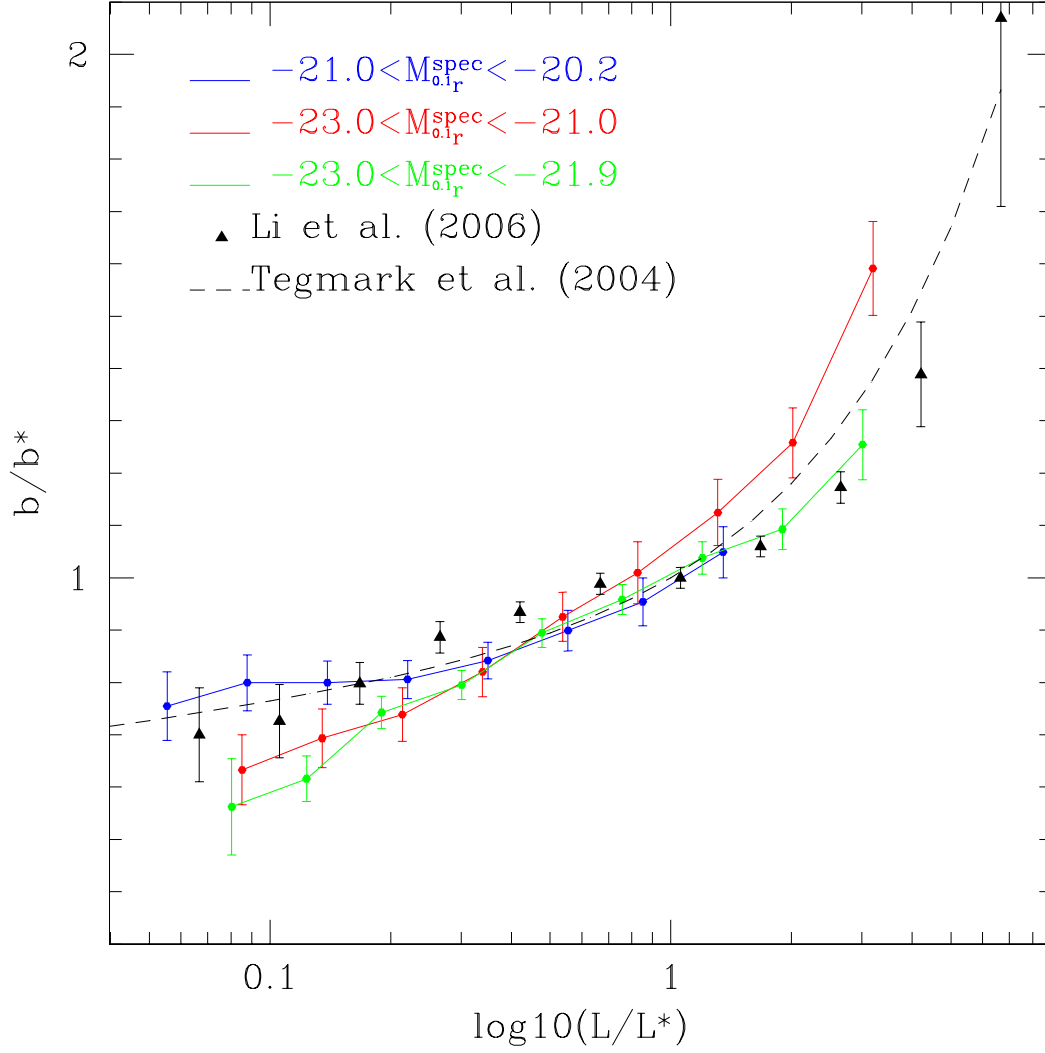


Fig. 12.— Relative bias factor as a function of luminosity, measured for low-redshift samples. Symbols and lines are similar as in Figure 10.